Activation of Liver X Receptor Inhibits Osteopontin and Ameliorates Diabetic Nephropathy

Hiromi Tachibana,* Daisuke Ogawa,*† Yuichi Matsushita,* Dennis Bruemmer,‡ Jun Wada,* Sanae Teshigawara,* Jun Eguchi,* Chikage Sato-Horiguchi,*† Haruhito Adam Uchida,* Kenichi Shikata,*§ and Hirofumi Makino*

Departments of *Medicine and Clinical Science and †Diabetic Nephropathy, Okayama University Graduate School of Medicine, Dentistry and Pharmaceutical Sciences, Okayama, Japan; ‡Division of Endocrinology and Molecular Medicine, University of Kentucky College of Medicine, Lexington, Kentucky; and §Center for Innovative Clinical Medicine, Okayama University Hospital, Okayama, Japan

ABSTRACT

Osteopontin is a proinflammatory cytokine and monocyte chemoattractant implicated in the pathogenesis of diabetic nephropathy. Synthetic agonists for liver X receptors (LXRs) suppress the expression of proinflammatory genes, including osteopontin, but whether LXR activation modulates diabetic nephropathy is unknown. We administered the LXR agonist T0901317 to mice with streptozotocin-induced diabetes and evaluated its effects on diabetic nephropathy. The LXR agonist decreased urinary albumin excretion without altering blood glucose levels and substantially attenuated macrophage infiltration, mesangial matrix accumulation, and interstitial fibrosis. LXR activation suppressed the gene expression of inflammatory mediators, including osteopontin, in the kidney cortex. *In vitro*, LXR activation suppressed osteopontin expression in proximal tubular epithelial cells by inhibiting AP-1–dependent transcriptional activation of the osteopontin promoter. Taken together, these results suggest that inhibition of renal osteopontin by LXR agonists may have therapeutic potential for diabetic nephropathy.

J Am Soc Nephrol 23: 1835–1846, 2012. doi: 10.1681/ASN.2012010022

Osteopontin (OPN) is a secreted extracellular matrix protein and proinflammatory cytokine that has been identified as a key component of cell-mediated immunity.[1] It is abundantly secreted by macrophages, and it mediates their recruitment and activation at sites of inflammation by regulating monocyte adhesion, migration, and inflammatory gene expression.[2,3] OPN is expressed in atherosclerotic lesions, where it is abundantly synthesized by macrophages and to lesser extents, smooth muscle cells and endothelial cells.[4] Using murine models, we and others have shown decreased atherosclerosis and macrophage accumulation in OPN-deficient mice,[5,6] identifying OPN as a potential target for pharmacological intervention in atherosclerosis. In humans, the plasma OPN level is significantly correlated with the extent of coronary atherosclerosis.[7,8] Moreover, the OPN levels are particularly elevated in patients with type 2 diabetes,[9,10] and we showed that peroxisome proliferator-activated receptor α ligands suppress OPN expression in macrophages *in vitro* and that bezafibrate reduces plasma OPN levels in patients with type 2 diabetes.[11] These clinical studies provide evidence that OPN may play a causal role in the development of cardiovascular disease in humans.

OPN is highly expressed in the kidney interstitium in models of diabetic nephropathy.[12,13] Because OPN is a macrophage chemotactic protein, OPN expression and macrophage accumulation

Received January 13, 2012. Accepted July 5, 2012.

Published online ahead of print. Publication date available at www.jasn.org.

Correspondence: Dr. Daisuke Ogawa, Department of Medicine and Clinical Science, Okayama University Graduate School of Medicine, Dentistry and Pharmaceutical Sciences, 2-5-1 Shikata-cho, Kita-ku, Okayama 700-8558, Japan. Email: daiogawa@md.okayama-u.ac.jp

may play a role in the tubulointerstitial injury in diabetic nephropathy in rats[13,14] and mice.[15,16] Moreover, we and others have shown by DNA microarray studies that OPN gene expression is upregulated in the renal cortex and correlated with the degree of albuminuria in diabetic nephropathy,[16–18] suggesting that regulation of OPN expression could be a potential target for therapeutic intervention in diabetic nephropathy. Furthermore, albuminuria and renal damage are ameliorated in OPN-deficient diabetic mice,[19,20] also supporting the notion that OPN may be causally involved in the pathogenesis of diabetic nephropathy.

Liver X receptors (LXRs) are important regulators of cholesterol, free fatty acid, and glucose metabolism.[21] In addition to their importance in lipid and glucose metabolism, LXR activation was recently found to regulate immune processes and inhibit inflammatory gene expression in macrophages.[22,23] Synthetic LXR agonists were shown to prevent atherosclerosis in murine models and inhibit inflammation.[22,24] We showed that LXR ligands T0901317 and GW3965 inhibit cytokine-induced OPN expression in macrophages.[25] These effects are mediated by inhibition of the c-Jun/c-Fos DNA-binding activities to the proximal OPN promoter, which impairs activator protein-1 (AP-1)–dependent OPN transcription.[25] These findings define a novel mechanism, where LXR ligands may impact macrophage inflammatory responses and atherosclerosis. However, the effects of LXR ligands on OPN expression in diabetic nephropathy remain unclear.

The purpose of the present study was to investigate the hypothesis that LXR activation prevents the development of diabetic nephropathy by inhibiting OPN expression and macrophage infiltration in the kidney interstitium.

RESULTS

LXR Ligand Ameliorates Diabetic Nephropathy

The metabolic data are summarized in Table 1. At 8 weeks after diabetes induction by streptozotocin (STZ), there were no significant differences in the systolic BPs, kidney weights, and triglyceride levels between the three groups of nondiabetic control mice (control), STZ-induced diabetic mice (DM), and diabetic mice treated with LXR agonist T0901317 (DM +T0901317). Hemoglobin A1c (HbA1c) was significantly higher in the DM group than the control group, but there was no significant difference between the DM and DM+T0901317 groups. Urinary albumin excretion (UAE) increased in the diabetic mice during the study. However, T0901317 treatment significantly reduced the mean UAE compared with the DM group at 8 weeks after diabetes induction. Representative glomeruli in periodic acid–methenamine silver (PAM) -stained sections are shown in Figure 1A. Glomerular hypertrophy and mesangial matrix expansion were observed in the DM group at the end of the 8-week observation period. However, these changes were ameliorated in the DM+T0901317 group compared with the DM group (Figure 1B). Interstitial fibrosis was examined in Masson's trichrome-stained renal sections (Figure 1C). The fibrotic area in the interstitium was larger in the DM group than the control group. The fibrotic area was markedly reduced in the DM+T0901317 group compared with the DM group (Figure 1D). Because LXR activation is known to increase lipogenesis, we measured the triglyceride levels and expressions of lipogenic enzymes, including sterol regulatory element-binding protein 1c (SREBP-1c), acetyl-coenzyme A carboxylase α, and fatty acid synthase. As shown in Supplemental Figure 1A, the gene expressions of SREBP-1c and acetyl-coenzyme A carboxylase α were increased in the DM+T0901317 group compared with the DM group. However, there were no significant differences in the triglyceride levels in serum (Table 1) and renal tissues (Supplemental Figure 1B) between the control, DM, and DM+T0901317 groups.

Table 1. Metabolic data at 8 weeks after the induction of diabetes

	Control (n=8)	DM (n=8)	DM+T0901317 (n=8)
Systolic BP (mmHg)	102.7±6.7	115.9±3.8	113.2±2.7
HbA1c (%)	4.25±0.05	9.03±0.46[a]	9.14±0.46[a]
Body weight (g)	26.57±0.35	18.66±1.23[a]	20.23±0.79[a]
Kidney weight (mg)	273.7±7.3	311.3±20.0	278.6±10.1
Relative kidney weight (mg/g body weight)	11.23±0.46	17.22±1.54[a]	13.86±0.52[b]
Triglycerides (mg/dl)	25.3±2.1	43.0±14.7	42.9±8.1
UAE (μg/24 h)	9.3±1.2	82.8±11.7[a]	52.9±7.5[a,b]

Data are means ± SEM. Control, nondiabetic control mice; DM, untreated diabetic mice; DM+T0901317, T0901317-treated diabetic mice; HbA1c, hemoglobin A1c; UAE, urinary albumin excretion.
[a]$P<0.01$ versus the control group.
[b]$P<0.01$ versus the DM group.

LXR Ligand Inhibits Macrophage Infiltration in the Kidney

The number of macrophages in the glomeruli was remarkably higher in the DM group than the control group. Interestingly, the macrophage infiltration into the glomeruli was significantly reduced in the DM+T0901317 group compared with the DM group (Figure 2, A and B). Similarly, the macrophage infiltration into the interstitium was increased in the DM group but suppressed in the DM+T0901317 group (Figure 2, A and 2C).

LXR Agonist Suppresses Diabetes-Induced OPN Expression in the Kidney

We detected OPN mRNA and protein expressions in the kidneys. At 8 weeks, renal OPN mRNA expression was significantly higher in the DM group than the control group (Figure 3A). Immunoperoxidase staining and Western blotting analysis also revealed that OPN protein expression in the kidney was significantly upregulated in the DM group compared with the control group (Figure 3, B and C). Treatment with T0901317 resulted in substantial suppression of the diabetes-induced OPN mRNA and protein expressions.

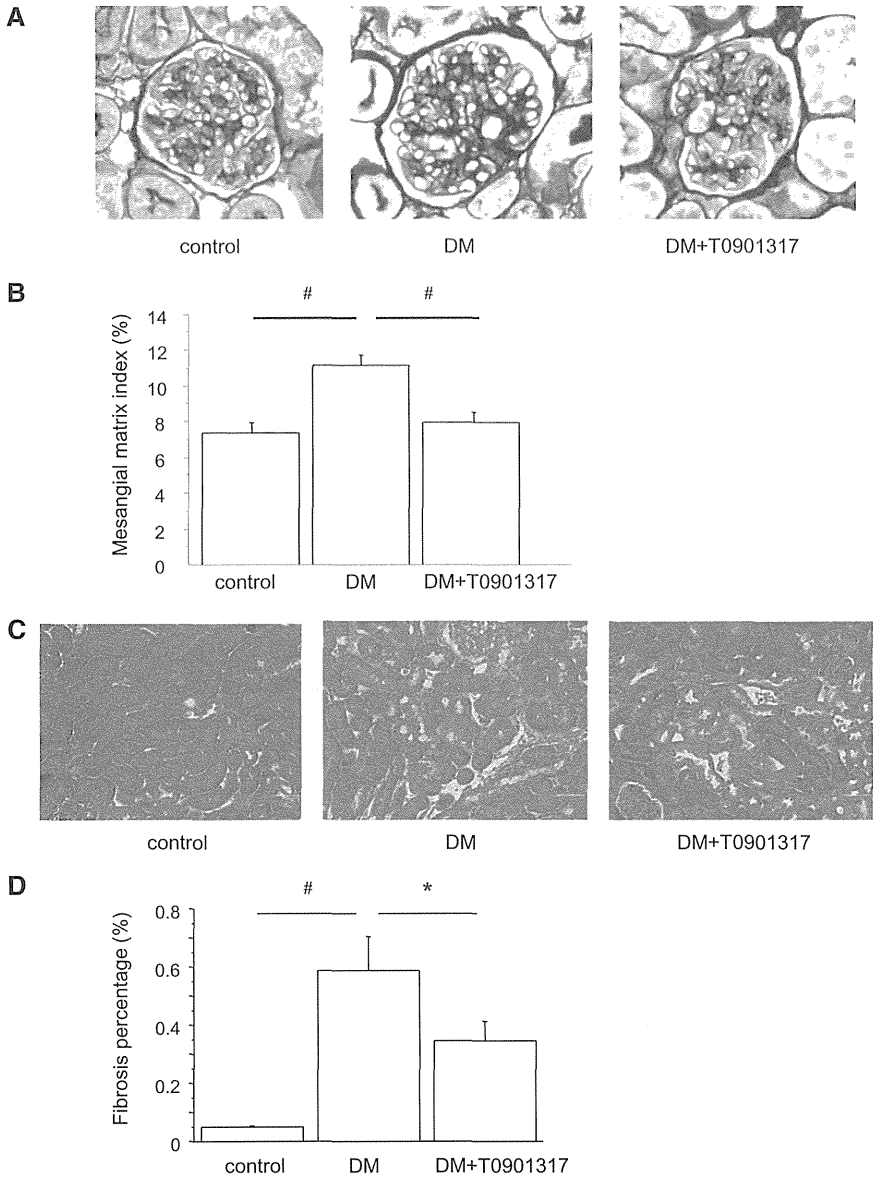

Figure 1. PAM staining and Masson's trichrome staining of kidney sections. (A) Representative glomeruli of PAM-stained kidneys from control, DM, and DM +T0901317 mice. Glomerular hypertrophy and mesangial matrix expansion are evident in the DM group. Original magnification, ×400. (B) MMI in glomeruli. T0901317 suppresses the increase in the MMI compared with the DM group. Data are means ± SEM. *P<0.001. (C) Representative photomicrographs of kidney sections with Masson's trichrome staining. Interstitial fibrosis is significantly increased in the DM group compared with the control group and significantly decreased in the DM+T0901317 group compared with the DM group. Original magnification, ×400. (D) Percentages of fibrosis in glomeruli. Data are means ± SEM. #P<0.001, *P<0.05.

Macrophage and Inflammatory Gene Expressions in the Renal Cortex

Quantitative RT-PCR (qRT-PCR) analyses of the kidney tissues revealed that the expression levels of two macrophage marker genes, CD14 and CD11c, were increased in the DM group and that T0901317 treatment markedly reduced these gene expression levels (Figure 4). CD14 is a marker for all macrophages, whereas CD11c is specific for the proinflammatory (M1) subtype of macrophages. Similarly, diabetes induction increased the renal expressions of several proinflammatory and proatherogenic genes, including monocyte chemoattractant protein 1 (MCP-1), TNF-α, TGF-β, and intracellular adhesion molecule 1 (ICAM-1). Although T0901317 decreased the expressions of MCP-1, TNF-α, and TGF-β, it had no effect on ICAM-1 expression (Figure 4). Similar to OPN, MCP-1 is a key chemokine involved in macrophage recruitment, and it plays a significant role in diabetic nephropathy.[26,27] TNF-α and TGF-β are also critical inflammatory cytokines involved in diabetic nephropathy.[28,29] Collectively, these data indicate that the LXR agonist T0901317 inhibits diabetes-induced macrophage recruitment and inflammatory gene expression in the kidney.

LXR Agonist Inhibits OPN Expression in Proximal Tubular Epithelial Cells

Our *in vivo* studies showed that diabetes-induced OPN expression in the kidney interstitium was suppressed by T0901317 treatment. Based on these data, we analyzed whether T0901317 modulates OPN expression in mProx24 cells, a mouse proximal tubular epithelial cell line. qRT-PCR experiments showed that high glucose-induced OPN mRNA expression was dose-dependently suppressed by T0901317 (Figure 5A), indicating that OPN suppression in mProx24 cells by the LXR ligand occurs at the gene expression level. Similarly, pretreatment of mProx24 cells with T0901317 resulted in dose-dependent inhibition of OPN protein expression (Figure 5B).

LXR Ligand Suppresses OPN Transcription

To further analyze the effects of the LXR ligand on OPN transcription, we transiently transfected mProx24 cells with a 2-kb OPN promoter fragment. High-glucose stimulation resulted in significant induction of OPN promoter activity, which was suppressed by T0901317 (Figure 6A). The inhibition of OPN promoter activity by T0901317 was dose-dependent, and it paralleled the inhibition of OPN mRNA and protein expressions. These findings suggest that the LXR ligand suppresses high glucose-induced OPN expression by inhibiting OPN gene transcription. To confirm the specificity of T0901317 for LXRα and LXRβ, we

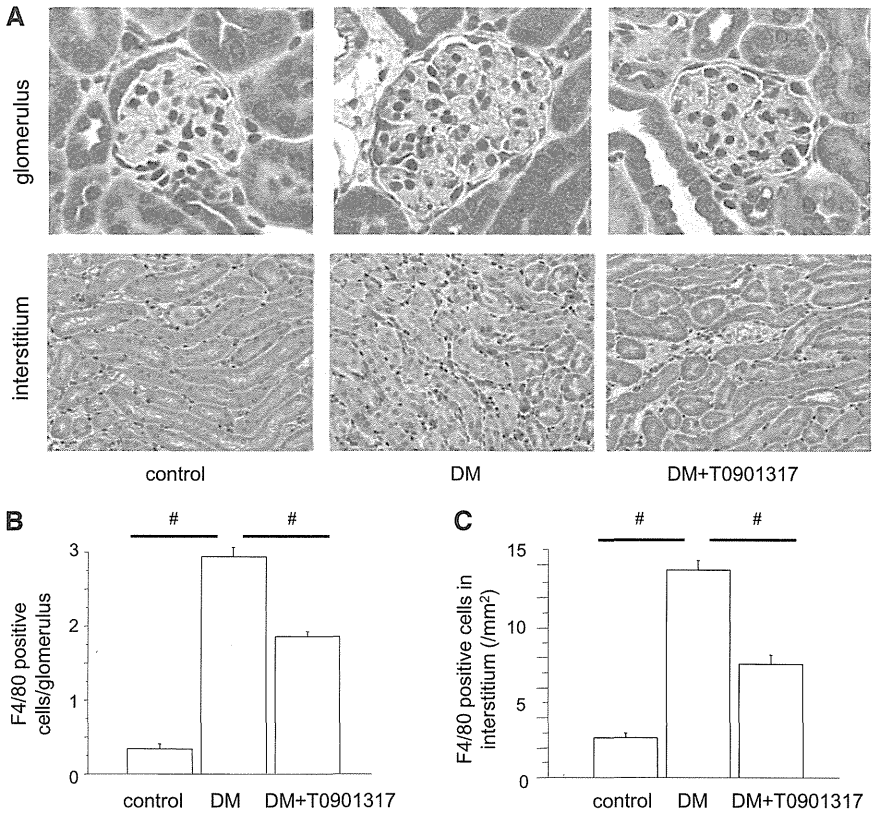

Figure 2. Macrophage infiltration into the kidney. (A) The macrophage infiltration into the glomeruli and interstitium is remarkable in the DM group and suppressed in the DM +T0901317 group. Original magnification, ×400. (B) Numbers of intraglomerular macrophages. Data are means ± SEM. $^{\#}P<0.001$. (C) Numbers of macrophages in the interstitium. Data are means ± SEM. $^{\#}P<0.001$.

performed small interfering RNA (siRNA) experiments (Supplemental Figure 2A). High glucose-induced OPN mRNA expression was suppressed by T0901317 in mProx24 cells transfected with a scrambled siRNA, and this suppression was canceled by both LXRα siRNA and LXRβ siRNA (Supplemental Figure 2B). These findings suggest that inhibition of OPN promoter activity by T0901317 is mediated by both LXRα and LXRβ.

Proximal OPN Promoter Confers Transcriptional Regulation of OPN in Proximal Tubular Epithelial Cells

To identify the promoter elements that regulate high glucose-induced OPN gene transcription and mediate transcriptional suppression of OPN in mProx24 cells by the LXR agonist, we used a series of 5′-deletion constructs (Figure 6B). Although the high glucose-induced transcriptional activity of the −83OPN-Luc promoter construct was completely suppressed by T0901317, the −61OPN-Luc construct was not inducible by high-glucose stimulation and exhibited transcriptional activity that was only slightly above the background signal. These findings indicate that the basal and high glucose-induced OPN promoter activity in mProx24 cells is dependent on transcription factor-binding sites located between −83 and −61 relative to the transcription initiation site.

LXR Agonist Suppresses OPN Promoter Activity by Negatively Interfering with AP-1–Dependent Transactivation of the OPN Promoter

Based on our previous study showing an important role of the AP-1 site located at −76 from the transcription initiation site for regulation of the OPN promoter in macrophages,[25] we generated a site-directed mutation in this AP-1 consensus element. Transient transfection of mProx24 cells with the OPN wild-type promoter construct and treatment with the LXR ligand T0901317 resulted in almost complete inhibition of OPN transcription (Figure 6C). In marked contrast, the OPN promoter construct bearing the mutated AP-1 site exhibited low basal activity, and it was not induced by high glucose. To further confirm an important role for this AP-1 site in the inhibition of OPN promoter activity by T0901317, we cotransfected mProx24 cells with the wild-type OPN reporter construct and eukaryotic expression vectors for c-Fos and c-Jun (Figure 6D). Overexpression of c-Fos and c-Jun resulted in complete loss of the ability of T0901317 to inhibit the high glucose-induced OPN promoter activity. To further corroborate the observation that the LXR ligand suppresses AP-1–dependent transactivation, we performed transfection experiments using a heterologous promoter driven by multiple AP-1 response elements. The high glucose-induced transcriptional activity of this AP-1–driven reporter construct was dose-dependently inhibited by T0901317 (Figure 6E). Taken together, these findings suggest that the suppression of the high glucose-induced OPN promoter activity by the LXR ligand is mediated through negative interference with c-Fos/c-Jun acting on the proximal OPN promoter.

LXR Ligand Inhibits AP-1 Binding to the Proximal OPN Promoter

Chromatin immunoprecipitation (ChIP) assays using a primer pair covering the AP-1 site at −76 in the OPN promoter were performed to confirm that the LXR ligand interferes with c-Fos and phospho-c-Jun binding to the endogenous OPN promoter. As shown in Figure 7, high-glucose stimulation of mProx24 cells resulted in binding of c-Fos and phospho-c-Jun to the AP-1 site at −76 relative to the endogenous OPN promoter, an effect that was inhibited by T0901317. Therefore, the suppression of the high glucose-induced binding to the AP-1 site at −76 by the LXR ligand reflects, at least in part, the inhibition of c-Fos and c-Jun expressions.

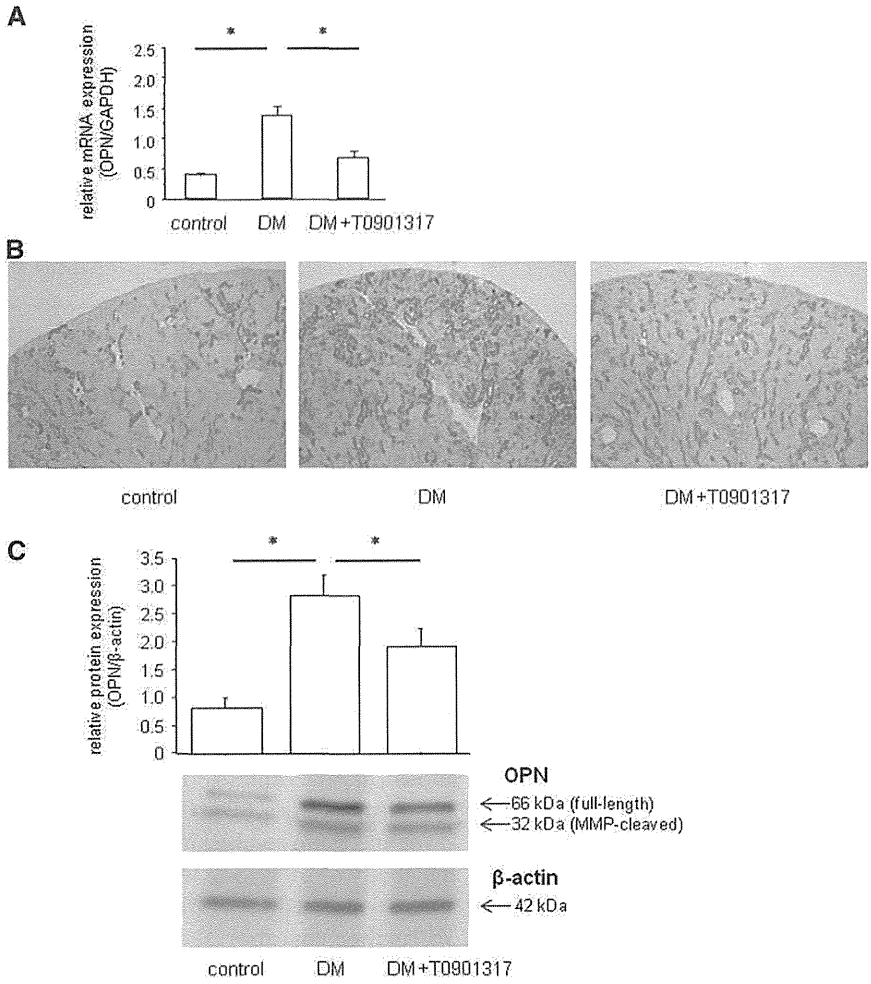

Figure 3. LXR agonist suppresses diabetes-induced OPN mRNA and protein expressions in the kidney. (A) Total RNA was isolated from the kidney samples and analyzed for the OPN mRNA expression levels by qRT-PCR. Renal OPN mRNA expression is significantly increased in the DM group compared with the control group. The OPN expression was normalized by the GAPDH expression. Data are means ± SEM. *$P<0.05$. (B) Localization of renal OPN protein by immunohistochemistry. OPN protein is predominantly localized in the interstitium of the kidney in the DM group, and its expression is suppressed in the DM+T0901317 group compared with the DM group. Original magnification, ×400. (C) Western blotting analysis of OPN protein expression. Full-length OPN as well as the C-terminal fragment of MMP-cleaved OPN are significantly upregulated in the DM group compared with the control group, and they are suppressed in the DM+T0901317 group compared with the DM group. Quantification was performed by densitometry of three independently performed experiments, with normalization by β-actin. Data are means ± SEM. *$P<0.05$.

DISCUSSION

LXR signaling pathways have recently been proposed as potential targets for therapeutic interventions in cardiovascular diseases.[21,30] However, the effects of LXR agonists on diabetic nephropathy have not been elucidated. In the present study, we have shown that the LXR agonist T0901317 ameliorated albuminuria, glomerular mesangial expansion, and interstitial fibrosis without affecting blood glucose and triglyceride levels in STZ-induced diabetic mice. T0901317 treatment markedly decreased the expression of OPN, a key proinflammatory cytokine in diabetic nephropathy, macrophage infiltration, and expressions of inflammatory genes, including MCP-1, TNF-α, and TGF-β, in the diabetic kidney. Furthermore, *in vitro* experiments using renal proximal tubular epithelial cells revealed that high glucose induced OPN expression and that T0901317 inhibited this OPN expression. This inhibition was mediated by inhibition of AP-1–dependent transcriptional activation of the OPN promoter. These observations further support an important role for LXR agonists in suppressing the inflammatory responses in diabetic kidneys and preventing the development of nephropathy.

Accumulating evidence has shown that a chronic low-grade state of inflammation plays an important role in the pathogenesis of diabetic nephropathy.[31,32] OPN is a proinflammatory cytokine implicated in the chemoattraction of monocytes and development of diabetic nephropathy,[16,17] and its levels are significantly elevated in patients with diabetic nephropathy.[9,33] OPN transcription is induced in response to high glucose,[34] raising the possibility that increased OPN secretion in diabetes may play a direct causal role in the development of diabetic nephropathy. For many years, it has been well known that OPN is upregulated in the interstitium, especially the proximal tubules, in the diabetic kidney.[12–14] Moreover, OPN deficiency prevents the development of diabetic nephropathy in murine models.[19,20] We recently reported that a peroxisome proliferator-activated receptor δ agonist, GW0742, attenuates diabetic nephropathy by suppressing inflammatory mediators, including OPN and MCP-1.[35] Therefore, OPN is regarded as a key molecule in the pathogenesis of diabetic nephropathy, and it may be a potential therapeutic target.

LXRs were first discovered as orphan receptors, and subsequently, they were identified as nuclear receptor targets of the cholesterol metabolites oxysterols. There are two LXRs encoded by distinct genes, namely LXRα, which is most highly expressed in the liver, adipose tissue, kidney, adrenal tissue, and macrophages, and LXRβ, which is ubiquitously expressed.[36] LXRα mRNA is widely expressed in the kidney and present in every nephron segment, including the glomeruli, and its activation by T0901317 mediates cholesterol efflux through ATP-binding cassette transporter A1 in cultured glomerular

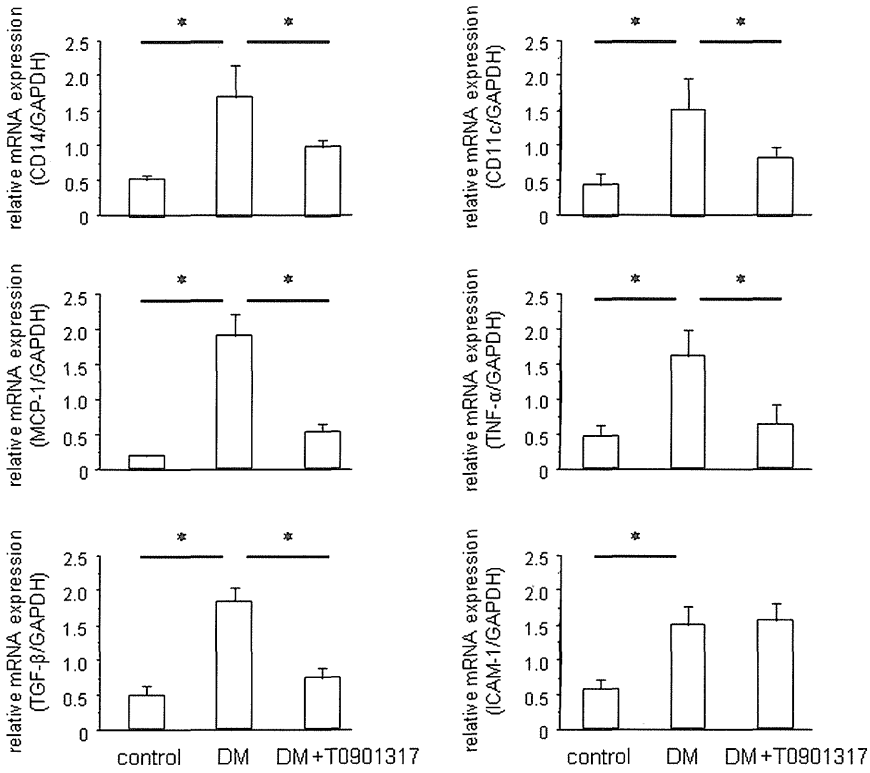

Figure 4. LXR activation suppresses diabetes-induced renal inflammation and macrophage infiltration. qRT-PCR analysis of the expressions of two macrophage markers, CD14 and CD11c, reveals that T0901317 inhibits diabetes-induced macrophage infiltration into the kidney. Similarly, T0901317 suppresses the MCP-1, TNF-α, and TGF-β mRNA levels in the kidney. The mRNA levels were normalized by the GAPDH mRNA level. Data are means ± SEM. *$P<0.05$.

mesangial cells.[37] Meanwhile, T0901317 increases the expression of stearoyl-CoA desaturase-1 through increased SREBP-1c in the proximal straight tubules.[38] These observations suggest that LXRs may play a role in regulating lipid metabolism and maintaining proximal tubule function. Although atheroprotective effects of LXR agonists have been reported,[22,24] there are no reports regarding the effects of LXR agonists on diabetic nephropathy.

Because the LXR ligand suppressed OPN expression and the OPN promoter analyses did not reveal the presence of any putative LXR response elements, the inhibition of the high glucose-induced OPN transcription by the LXR ligand probably involves an indirect mechanism through the regulation of other transcription factors that support OPN transcription. In this study, we identified an AP-1 consensus site in the OPN promoter located between −80 and −71 that supports the basal and induced transcriptional activity of the OPN promoter in proximal tubular epithelial cells. Using ChIP assays, we showed that the LXR agonist inhibited c-Fos and phospho-c-Jun binding to this AP-1 site in the proximal OPN promoter. The ability of the LXR ligand to suppress the OPN promoter activity was lost in cells overexpressing c-Fos and c-Jun. These findings, combined with our observation that the LXR ligand inhibited the transactivation of a heterologous AP-1–driven promoter, support the notion that LXR ligands suppress OPN expression by interfering with AP-1–dependent transactivation of the proximal OPN promoter.

Recent studies have suggested that OPN plays an important role in not only the interstitium but also the glomeruli. In the $Ins2^{Akita}$ mouse model of type 1 diabetic nephropathy, OPN immunostaining was increased in podocytes, and OPN knockout mice were protected against diabetes-induced albuminuria and mesangial expansion.[19] Furthermore, OPN deletion decreased albuminuria and the mesangial area in both type 1 ($Ins2^{Akita}$) and type 2 (*db/db*) diabetic mouse models, and recombinant OPN upregulated TGF-β expression and signaling in cultured mouse mesangial cells.[20] In the present study, glomerular hypertrophy, mesangial matrix expansion, and macrophage infiltration were observed in the diabetic glomeruli, and these changes were ameliorated by administration of T0901317. These findings suggest that LXR agonists may have beneficial effects in not only the interstitium but also the glomerular cells. Because LXRα and LXRβ are present in not only the interstitium but also the glomeruli,[37,39] T0901317 may suppress OPN expression and macrophage infiltration in the glomeruli and subsequently, alter glomerular hypertrophy and albuminuria. However, OPN expression was predominantly localized in the proximal tubular epithelial cells and to a lesser extent, the glomeruli of the diabetic kidneys. Therefore, we focused on the regulation of OPN expression in proximal tubular epithelial cells by an LXR agonist in this study, and additional investigations are needed.

There are several limitations to this study. The first limitation is the selectivity of T0901317 as an LXR agonist. Recent studies showed that T0901317 can activate not only LXRs but also other nuclear hormone receptors, including pregnane X receptor, farnesoid X receptor, and retinoic acid receptor-related orphan receptor-α/γ.[40–42] We showed that activation of both LXRα and LXRβ by T0901317 inhibited OPN expression in the present study. However, it remains possible that activation of other nuclear hormone receptors could suppress the OPN expression. Therefore, it is expected that highly selective LXR agonists will be developed.

The second limitation is that T0901317 has lipogenic effects. In this study, although the gene expressions of lipogenic enzymes were slightly increased after administration of T0901317, lipid accumulation in renal tissues and serum triglyceride elevation were not observed. There are several speculations of why T0901317 did not induce lipogenic activities. One

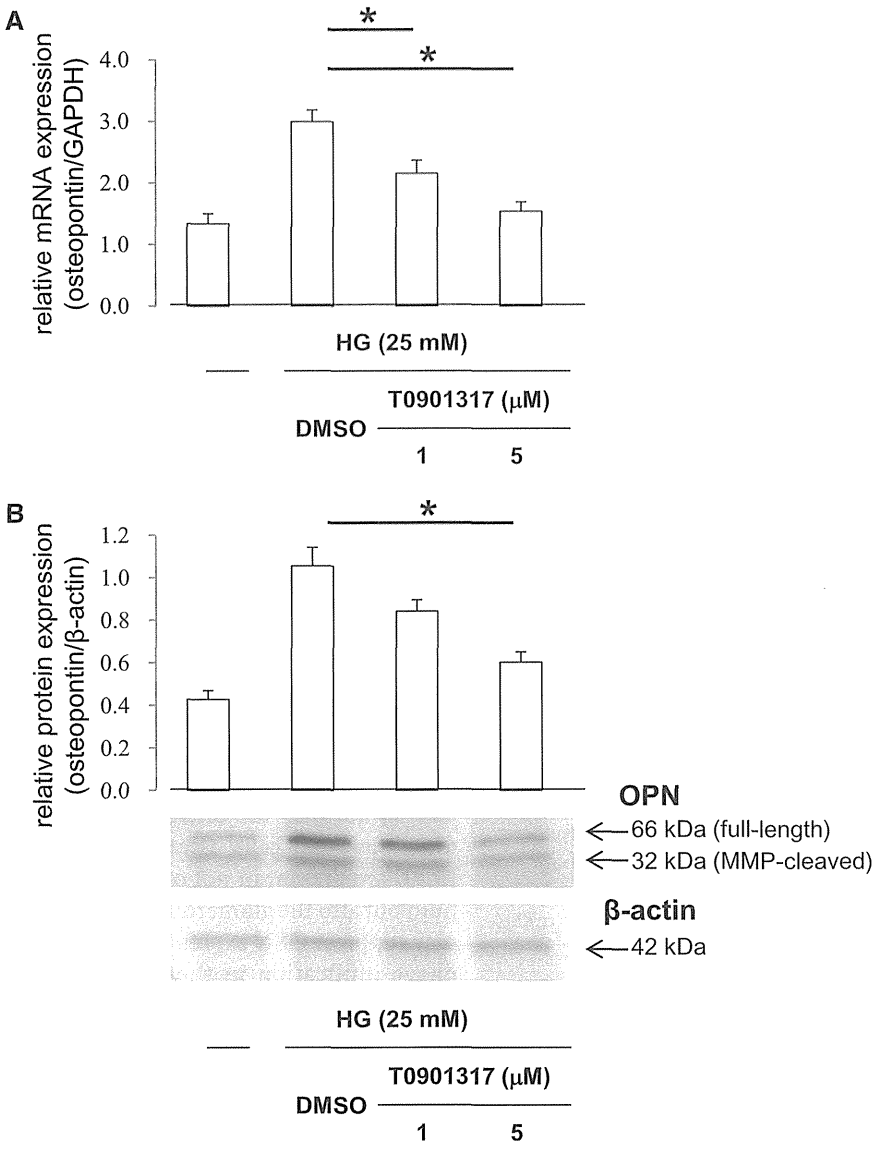

Figure 5. LXR agonist suppresses HG-induced OPN expression in proximal tubular epithelial cells. mProx24 cells, a mouse renal proximal tubular epithelial cell line, were pretreated for 24 h with vehicle (DMSO) or the indicated concentrations of the synthetic LXR agonist T0901317. (A) After stimulation for 24 h with high-glucose (HG) medium (25 mM), total RNA was isolated from mProx24 cells and analyzed for the OPN mRNA expression levels by qRT-PCR. Quantification was performed by densitometry, with normalization by the cohybridized GAPDH mRNA expression levels. Data are means ± SEM. *$P<0.05$. (B) After 24 h, OPN protein expression was analyzed by Western blotting. Full-length OPN as well as the C-terminal fragment of MMP-cleaved OPN are significantly upregulated by HG stimulation, and they are suppressed by pretreatment with T0901317. Quantification was performed by densitometry of three independently performed experiments, with normalization by β-actin. Data are means ± SEM. *$P<0.05$.

speculation is that insulin deficiency may strongly suppress the lipogenesis and lipid accumulation in the kidney because of two reasons: we used STZ to induce diabetes, and insulin was defective in this model. Another speculation involves the LXR downregulation by diabetes induction (Supplemental Figure 1C). These findings are consistent with a previous study analyzing the expressions of LXRs in other type 1 diabetes models.[43] This downregulation of LXRs may be involved in weakening the lipogenic effects of T0901317. A third speculation is the amount of T0901317. Many investigators used T0901317 at 50 mg/kg per day and observed lipogenic effects in previous studies.[44–48] To avoid severe hepatic lipogenesis, we used a comparatively low dose (10 mg/kg per day) in this study. Recently, T0901317 and a new steroidal LXR agonist, DMHCA, were reported to decrease the activity of intestinal and renal sodium gradient-dependent phosphate transporters, and the gene expressions of lipogenic enzymes with DMHCA were lower than those gene expressions after activation by T0901317.[49] Additional studies are required to address whether the generation of selective LXR modulators will circumvent lipogenesis and provide a novel strategy for treating diabetic nephropathy.

In conclusion, the present data show that the LXR agonist T0901317 shows renoprotective effects through its anti-inflammatory activity by inhibiting OPN expression and macrophage infiltration in the diabetic kidney. Because OPN is a key component in the inflammatory response and recruitment of monocytes/macrophages into the diabetic kidney, inhibition of OPN expression by LXR agonists could be a therapeutic target in human diabetic nephropathy.

CONCISE METHODS

Experimental Protocol

Male C57BL/6J mice were purchased from Charles River (Yokohama, Japan). At 8 weeks of age, the mice were divided into three groups: nondiabetic control mice (control; $n=8$), STZ-induced diabetic mice (DM; $n=8$), and diabetic mice treated with the LXR agonist T0901317 (DM+T0901317; $n=8$). T0901317 was purchased from Sigma-Aldrich (Tokyo, Japan). Diabetes was induced by peritoneal injection of 200 mg/kg STZ (Sigma-Aldrich) in citrate buffer (pH 4.5). Blood glucose was measured by the glucose oxidase method at 3 and 7 days after the STZ injection, and only mice with blood glucose concentrations of >16 mmol/L were used in the study. The mice in the control group were injected with citrate buffer. The mice in the DM +T0901317 group received 10 mg/kg per day T0901317 by gavage for 8

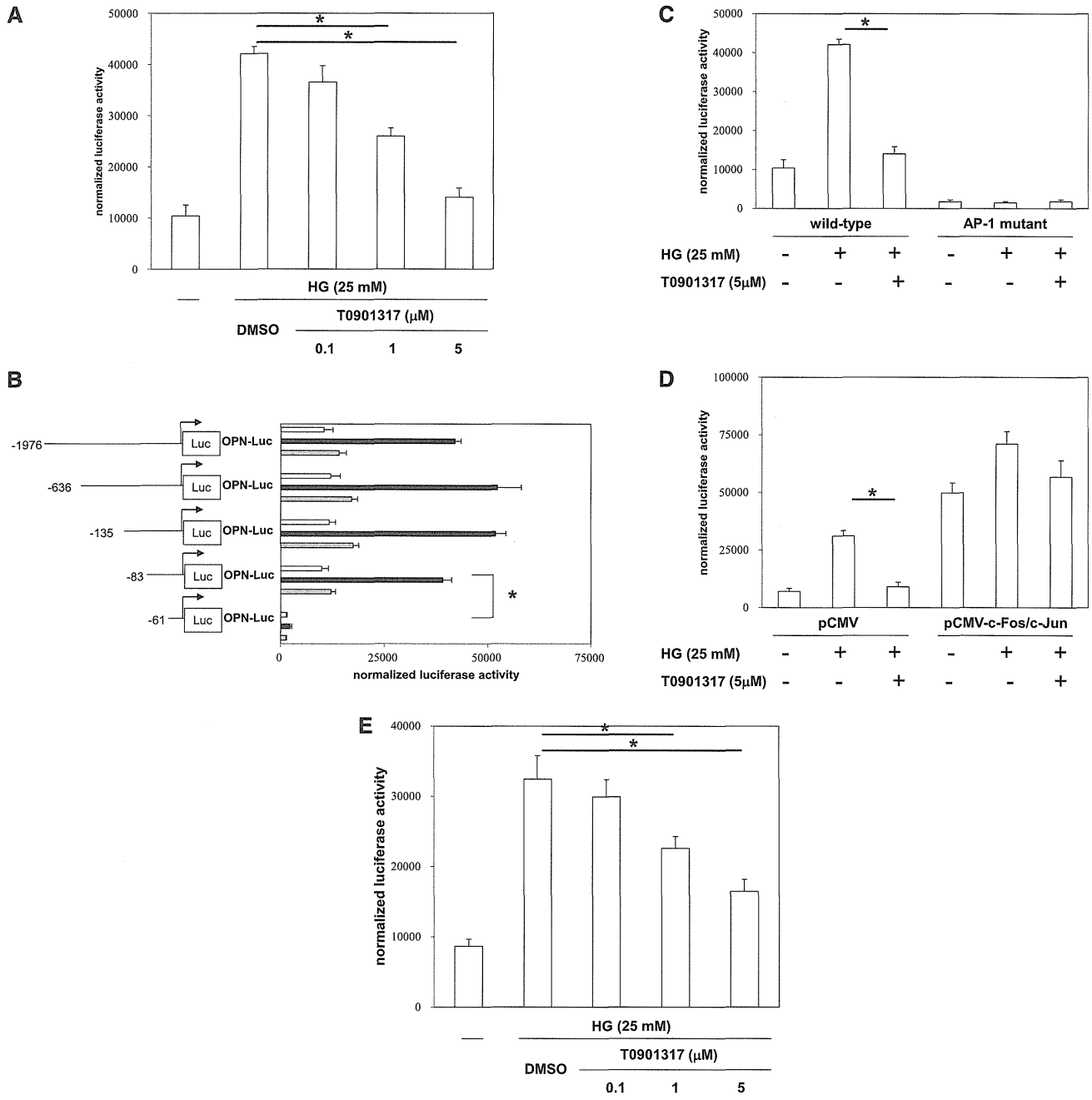

Figure 6. LXR agonist inhibits OPN promoter activity by negative interference with AP-1 signaling pathways. mProx24 cells were transiently transfected with a full-length OPN promoter construct. After the transfection, the cells were pretreated for 24 h with vehicle (DMSO) or the indicated concentrations of the synthetic LXR agonist T0901317 and stimulated for 24 h with high glucose (HG) medium (25 mM) as indicated. Data are expressed as the normalized luciferase activities. Data are means ± SEM. *$P<0.05$. (A) The transfected mProx24 cells were pretreated for 24 h with T0901317 and stimulated for 24 h with HG medium as indicated. The transfection efficiency was adjusted by normalization of the firefly luciferase activities by the *Renilla* luciferase activities generated by cotransfection with 10 ng pRL-CMV. (B) OPN promoter elements encoded by nucleotides −83 to −61 convey the transcriptional activity in mProx24 cells. mProx24 cells were transiently transfected with the indicated 5′-deletion constructs of the OPN promoter. The transfected mProx24 cells were left untreated (white bars) or incubated with vehicle (DMSO; black bars) or T0901317 (5 μmol/L; gray bars) for 24 h before stimulation with HG medium. (C) mProx24 cells were transiently transfected with the full-length wild-type or AP-1–mutated OPN promoter. (D) mProx24 cells were transfected with the OPN promoter construct alone or cotransfected with the OPN promoter construct and the empty pCMV vector (400 ng) or pCMV-c-Fos (200 ng) and pCMV-c-Jun (200 ng) expression vectors. (E) mProx24 cells were transfected with an AP-1–driven heterologous promoter.

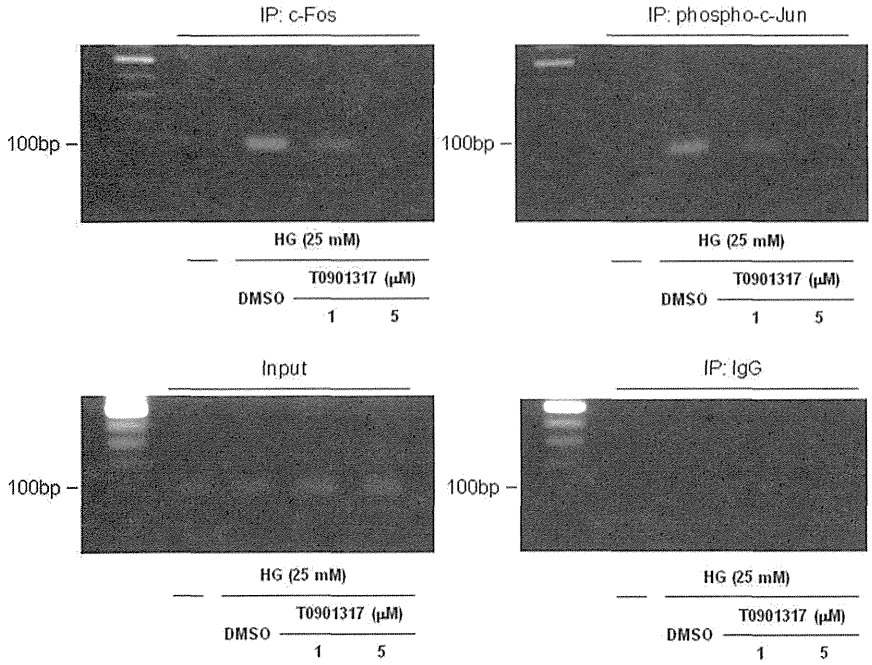

Figure 7. LXR agonist inhibits AP-1 binding to the proximal OPN promoter. mProx24 cells were pretreated for 24 h with vehicle (DMSO) or 1 or 5 μmol/L T0901317 and stimulated with HG medium (25 mM) for 24 h. ChIP assays were performed using anti–c-Fos and anti–phospho-c-Jun antibodies. Total extract (input) and rabbit IgG were used as controls. The ethidium bromide-stained agarose gels shown are representative of three independently performed experiments.

weeks. All mice had free access to a standard diet and tap water. All procedures were performed according to the Guidelines for Animal Experiments at Okayama University Medical School, Japanese Government Animal Protection and Management Law (Number 105), and Japanese Government Notification on Feeding and Safekeeping of Animals (Number 6). The mice were euthanized at 8 weeks after diabetes induction. The kidneys were removed, weighed, and fixed in 10% formalin for PAM staining and Masson's trichrome staining. Parts of the remaining tissues were embedded in optimal cutting temperature compound (Sakura Finetechnical, Tokyo, Japan) and frozen immediately in acetone cooled on dry ice. Other tissues were snap-frozen in liquid nitrogen and stored at −80°C.

Metabolic Data

We measured the body weight, BP, HbA1c, 24 h UAE, and creatinine clearance at 0, 4, and 8 weeks. BP was measured using the tail-cuff method (Softron, Tokyo, Japan). HbA1c was measured using a high-pressure liquid chromatography method, and serum creatinine was measured using an enzymatic method. Urine was collected for 24 h with each mouse individually housed in a metabolic cage and provided food and water *ad libitum*. The urinary albumin concentration was measured as previously described.[50]

Light Microscopy

Sections (4 μm thick) cut from 10% formalin-fixed, paraffin-embedded kidney samples were subjected to PAM staining and Masson's trichrome staining. To evaluate the glomerular size, we examined 20 randomly selected glomeruli in the cortex per animal under high magnification (×400) at 8 weeks after the induction of diabetes. The areas of the glomerular tuft and mesangial matrix index (MMI) were measured using Lumina Vision software (Mitani Corporation, Tokyo, Japan). The MMI was defined as the PAM-positive area in the tuft area, and it was calculated using the following formula: MMI = PAM-positive area/tuft area. The results were expressed as means ± SE (per micrometer squared for the tuft area and arbitrary units for the MMI). The Masson's trichrome-stained sections were assessed for the proportion of fibrosis in the kidney tissues using a computer image analysis system as described above.

Immunoperoxidase Staining

Immunoperoxidase staining was performed as previously described.[50] Briefly, fresh-frozen sections were cut to 4-μm thickness using a cryostat. To evaluate the macrophage infiltration, we applied a rat anti-mouse monocyte/macrophage (F4/80) monoclonal antibody (ab6640; Abcam, Tokyo, Japan) followed by a biotin-labeled goat anti-rat IgG antibody (ab6844; Abcam). The avidin–biotin coupling reaction was performed on the sections using a Vectastain Elite Kit (Vector Laboratories, Burlingame, CA). We examined 20 glomeruli per animal and counted the number of F4/80-positive cells. The mean numbers of positive cells per glomerulus and interstitial tissue (per millimeter squared) were used for the estimation. To evaluate OPN expression, a rabbit anti-OPN polyclonal antibody (ab8448; Abcam) was applied, and it was followed by a biotin-labeled donkey anti-rabbit IgG antibody (Jackson ImmunoResearch Laboratories, West Grove, PA).

PCR Assays for Gene Expression

RNA from the renal cortex was isolated after 8 weeks of treatment using an RNeasy Mini Kit (Qiagen, Valencia, CA). Single-stranded cDNA was synthesized from the extracted RNA using a GeneAmp RNA PCR Core Kit (Applied Biosystems, Foster City, CA). To evaluate the mRNA expressions of OPN, CD14, CD11c, MCP-1, TNF-α, TGF-β, and ICAM-1 in the renal cortex, qRT-PCR was performed using a StepOnePlus Real-Time PCR System (Applied Biosystems) and SYBR Premix Ex Taq II (Takara Bio Inc., Otsu, Japan). The primers were purchased from Takara Bio Inc. and are listed in Table 2. Each sample was analyzed in triplicate and normalized by the glyceraldehyde-3-phosphate dehydrogenase (GAPDH) mRNA expression.

Western Blot Analysis

Western blotting was performed as previously described.[35] Briefly, the proteins were eluted, resolved by SDS-PAGE, and transferred to nitrocellulose membranes. After blocking in 20 mM Tris·HCl (pH 7.6) containing 150 mM NaCl, 0.1% Tween-20, and 5% (wt/vol)

Table 2. Primers used for qRT-PCR

Gene	Sense	Antisense
OPN	TACGACCATGAGATTGGCAGTGA	TATAGGATCTGGGTGCAGGCTGTAA
CD14	GGGCTGCTCAAACTTTCAGAATCTA	AATTGAAAGCGCTGGACCAATC
CD11c	AGGTCTGCTGCTGCTGGCTA	GAAGTTCTCACTGGGCAACCTG
MCP-1	GCATCCACGTGTTGGCTCA	CTCCAGCCTACTCATTGGGATCA
TNF-α	GTTCTATGGCCCAGACCCTCAC	GGCACCACTAGTTGGTTGTCTTTG
TGF-β	GTGTGGAGCAACATGTGGAACTCTA	TTGGTTCAGCCACTGCCGTA
ICAM-1	CAATTCACACTGAATGCCAGCTC	CAAGCAGTCCGTCTCGTCCA
GAPDH	TGTGTCCGTGGATCTGA	TTGCTGTTGAAGTCGCAGGAG

nonfat dried milk, the membranes were incubated with an anti-OPN antibody (ab8448; Abcam). This antibody recognizes full-length OPN (which appears at 66 kD on Western blotting) as well as the C-terminal fragment of matrix metalloproteinase (MMP) -cleaved OPN (which appears at 32 kD on Western blotting).[51] The membranes were hybridized with an anti–β-actin antibody (ab6276; Abcam) to monitor equivalent loading in different lanes. All experiments were repeated at least three times.

Cell Culture and Treatment

mProx24 cells, a mouse renal proximal tubular epithelial cell line, were cultured in DMEM supplemented with 5.5 mM D-glucose, 10% FBS, 100 U/mL penicillin, 100 mg/mL streptomycin, and 2 mM L-glutamine. For ligand treatment, the cells were serum-starved by culture in medium containing 0.5% FBS for 24 h. After pretreatment with T0901317 for 24 h, the cells were stimulated with 25 mM D-glucose (high glucose) for 24 h. Individual experiments were repeated at least three times with different lots or preparations of cells. OPN mRNA and protein expressions in mProx24 cells were measured by qRT-PCR and Western blotting, respectively, as described above.

Plasmids and Transient Transfections

The OPN promoter constructs, AP-1 luciferase reporter construct, and c-Fos and c-Jun expression vectors were used as previously described.[25,34] The AP-1 site at −76 in the 2-kb OPN promoter construct was mutated from $^{-80}$CCTCATGAC^{-71} to $^{-80}$CGGCGGGAC^{-71} as previously described.[25] mProx24 cells were transfected with 1 μg DNA using a Neon Transfection System (Invitrogen, Carlsbad, CA). At 8 h after transfection, the cells were cultured in DMEM supplemented with 0.5% FBS in the presence of specified concentrations of T0901317 for 12 h before high-glucose stimulation. The luciferase activity was assayed after 24 h of stimulation using a Dual-Luciferase Reporter Assay System (Promega, Madison, WI) as previously described.[25] All experiments were repeated at least three times and in triplicate with different cell preparations.

ChIP Assays

ChIP assays were performed using a ChIP-IT Express (Active Motif, Carlsbad, CA) according to the manufacturer's instructions. Soluble chromatin was prepared from mProx24 cells treated with 1 or 5 μmol/L T0901317 for 24 h followed by stimulation with high glucose (25 mM) for 24 h. Chromatin was immunoprecipitated with antibodies (2 mg) directed against c-Fos (sc-8047; Santa Cruz Biotechnology, Santa Cruz, CA) and phospho-c-Jun (sc-822; Santa Cruz Biotechnology). The final DNA extracts were amplified by PCR using a primer pair that covered the AP-1 consensus sequence at −76 in the OPN promoter to yield a 151-bp PCR product (forward, 5′-ACCACAAAACCAGAGGAGGA-3′ and reverse, 5′-TTCAGTGTGAGCTGCTGGTG-3′).

Statistical Analyses

All values are presented as means ± SEM. The statistical significance of differences between groups was analyzed using one-way ANOVA followed by Scheffé's test. Values of $P<0.05$ were considered statistically significant.

ACKNOWLEDGMENTS

The authors thank Noriko Yamamoto and Yoshiko Hada for technical support.

This study was supported in part by Grants-in-Aid for Young Scientists (B) 21790813 and 23790942 from the Ministry of Education, Culture, Sports, Science, and Technology of Japan (to D.O.) and a Grant-in-Aid for Diabetic Nephropathy from the Ministry of Health, Labour, and Welfare of Japan. This work also received support from the Takeda Science Foundation, the Naito Foundation, and the Ryobi Teien Memory Foundation.

DISCLOSURES

None.

REFERENCES

1. Ashkar S, Weber GF, Panoutsakopoulou V, Sanchirico ME, Jansson M, Zawaideh S, Rittling SR, Denhardt DT, Glimcher MJ, Cantor H: Eta-1 (osteopontin): An early component of type-1 (cell-mediated) immunity. *Science* 287: 860–864, 2000
2. Denhardt DT, Giachelli CM, Rittling SR: Role of osteopontin in cellular signaling and toxicant injury. *Annu Rev Pharmacol Toxicol* 41: 723–749, 2001
3. Giachelli CM, Steitz S: Osteopontin: A versatile regulator of inflammation and biomineralization. *Matrix Biol* 19: 615–622, 2000
4. Giachelli CM, Bae N, Almeida M, Denhardt DT, Alpers CE, Schwartz SM: Osteopontin is elevated during neointima formation in rat arteries and is a novel component of human atherosclerotic plaques. *J Clin Invest* 92: 1686–1696, 1993
5. Bruemmer D, Collins AR, Noh G, Wang W, Territo M, Arias-Magallona S, Fishbein MC, Blaschke F, Kintscher U, Graf K, Law RE, Hsueh WA: Angiotensin II-accelerated atherosclerosis and aneurysm formation is attenuated in osteopontin-deficient mice. *J Clin Invest* 112: 1318–1331, 2003
6. Matsui Y, Rittling SR, Okamoto H, Inobe M, Jia N, Shimizu T, Akino M, Sugawara T, Morimoto J, Kimura C, Kon S, Denhardt D, Kitabatake A, Uede T: Osteopontin deficiency attenuates atherosclerosis in female apolipoprotein E-deficient mice. *Arterioscler Thromb Vasc Biol* 23: 1029–1034, 2003

7. Ohmori R, Momiyama Y, Taniguchi H, Takahashi R, Kusuhara M, Nakamura H, Ohsuzu F: Plasma osteopontin levels are associated with the presence and extent of coronary artery disease. *Atherosclerosis* 170: 333–337, 2003
8. Minoretti P, Falcone C, Calcagnino M, Emanuele E, Buzzi MP, Coen E, Geroldi D: Prognostic significance of plasma osteopontin levels in patients with chronic stable angina. *Eur Heart J* 27: 802–807, 2006
9. Yamaguchi H, Igarashi M, Hirata A, Tsuchiya H, Sugiyama K, Morita Y, Jimbu Y, Ohnuma H, Daimon M, Tominaga M, Kato T: Progression of diabetic nephropathy enhances the plasma osteopontin level in type 2 diabetic patients. *Endocr J* 51: 499–504, 2004
10. Takemoto M, Yokote K, Yamazaki M, Ridall AL, Butler WT, Matsumoto T, Tamura K, Saito Y, Mori S: Enhanced expression of osteopontin by high glucose. Involvement of osteopontin in diabetic macroangiopathy. *Ann N Y Acad Sci* 902: 357–363, 2000
11. Nakamachi T, Nomiyama T, Gizard F, Heywood EB, Jones KL, Zhao Y, Fuentes L, Takebayashi K, Aso Y, Staels B, Inukai T, Bruemmer D: PPARalpha agonists suppress osteopontin expression in macrophages and decrease plasma levels in patients with type 2 diabetes. *Diabetes* 56: 1662–1670, 2007
12. Fischer JW, Tschöpe C, Reinecke A, Giachelli CM, Unger T: Upregulation of osteopontin expression in renal cortex of streptozotocin-induced diabetic rats is mediated by bradykinin. *Diabetes* 47: 1512–1518, 1998
13. Kelly DJ, Wilkinson-Berka JL, Ricardo SD, Cox AJ, Gilbert RE: Progression of tubulointerstitial injury by osteopontin-induced macrophage recruitment in advanced diabetic nephropathy of transgenic (mRen-2)27 rats. *Nephrol Dial Transplant* 17: 985–991, 2002
14. Li C, Yang CW, Park CW, Ahn HJ, Kim WY, Yoon KH, Suh SH, Lim SW, Cha JH, Kim YS, Kim J, Chang YS, Bang BK: Long-term treatment with ramipril attenuates renal osteopontin expression in diabetic rats. *Kidney Int* 63: 454–463, 2003
15. Chow F, Ozols E, Nikolic-Paterson DJ, Atkins RC, Tesch GH: Macrophages in mouse type 2 diabetic nephropathy: Correlation with diabetic state and progressive renal injury. *Kidney Int* 65: 116–128, 2004
16. Susztak K, Böttinger E, Novetsky A, Liang D, Zhu Y, Ciccone E, Wu D, Dunn S, McCue P, Sharma K: Molecular profiling of diabetic mouse kidney reveals novel genes linked to glomerular disease. *Diabetes* 53: 784–794, 2004
17. Hsieh TJ, Chen R, Zhang SL, Liu F, Brezniceanu ML, Whiteside CI, Fantus IG, Ingelfinger JR, Hamet P, Chan JS: Upregulation of osteopontin gene expression in diabetic rat proximal tubular cells revealed by microarray profiling. *Kidney Int* 69: 1005–1015, 2006
18. Usui HK, Shikata K, Sasaki M, Okada S, Matsuda M, Shikata Y, Ogawa D, Kido Y, Nagase R, Yozai K, Ohga S, Tone A, Wada J, Takeya M, Horiuchi S, Kodama T, Makino H: Macrophage scavenger receptor-a-deficient mice are resistant against diabetic nephropathy through amelioration of microinflammation. *Diabetes* 56: 363–372, 2007
19. Lorenzen J, Shah R, Biser A, Staicu SA, Niranjan T, Garcia AM, Gruenwald A, Thomas DB, Shatat IF, Supe K, Woroniecki RP, Susztak K: The role of osteopontin in the development of albuminuria. *J Am Soc Nephrol* 19: 884–890, 2008
20. Nicholas SB, Liu J, Kim J, Ren Y, Collins AR, Nguyen L, Hsueh WA: Critical role for osteopontin in diabetic nephropathy. *Kidney Int* 77: 588–600, 2010
21. Tontonoz P, Mangelsdorf DJ: Liver X receptor signaling pathways in cardiovascular disease. *Mol Endocrinol* 17: 985–993, 2003
22. Joseph SB, Castrillo A, Laffitte BA, Mangelsdorf DJ, Tontonoz P: Reciprocal regulation of inflammation and lipid metabolism by liver X receptors. *Nat Med* 9: 213–219, 2003
23. Castrillo A, Joseph SB, Marathe C, Mangelsdorf DJ, Tontonoz P: Liver X receptor-dependent repression of matrix metalloproteinase-9 expression in macrophages. *J Biol Chem* 278: 10443–10449, 2003
24. Joseph SB, McKilligin E, Pei L, Watson MA, Collins AR, Laffitte BA, Chen M, Noh G, Goodman J, Hagger GN, Tran J, Tippin TK, Wang X, Lusis AJ, Hsueh WA, Law RE, Collins JL, Willson TM, Tontonoz P: Synthetic LXR ligand inhibits the development of atherosclerosis in mice. *Proc Natl Acad Sci U S A* 99: 7604–7609, 2002
25. Ogawa D, Stone JF, Takata Y, Blaschke F, Chu VH, Towler DA, Law RE, Hsueh WA, Bruemmer D: Liver x receptor agonists inhibit cytokine-induced osteopontin expression in macrophages through interference with activator protein-1 signaling pathways. *Circ Res* 96: e59–e67, 2005
26. Chow FY, Nikolic-Paterson DJ, Ozols E, Atkins RC, Rollin BJ, Tesch GH: Monocyte chemoattractant protein-1 promotes the development of diabetic renal injury in streptozotocin-treated mice. *Kidney Int* 69: 73–80, 2006
27. Chow FY, Nikolic-Paterson DJ, Ma FY, Ozols E, Rollins BJ, Tesch GH: Monocyte chemoattractant protein-1-induced tissue inflammation is critical for the development of renal injury but not type 2 diabetes in obese db/db mice. *Diabetologia* 50: 471–480, 2007
28. Navarro-González JF, Mora-Fernández C: The role of inflammatory cytokines in diabetic nephropathy. *J Am Soc Nephrol* 19: 433–442, 2008
29. Sharma K, Ziyadeh FN: Hyperglycemia and diabetic kidney disease. The case for transforming growth factor-beta as a key mediator. *Diabetes* 44: 1139–1146, 1995
30. Lund EG, Menke JG, Sparrow CP: Liver X receptor agonists as potential therapeutic agents for dyslipidemia and atherosclerosis. *Arterioscler Thromb Vasc Biol* 23: 1169–1177, 2003
31. Saraheimo M, Teppo AM, Forsblom C, Fagerudd J, Groop PH: Diabetic nephropathy is associated with low-grade inflammation in Type 1 diabetic patients. *Diabetologia* 46: 1402–1407, 2003
32. Nelson CL, Karschimkus CS, Dragicevic G, Packham DK, Wilson AM, O'Neal D, Becker GJ, Best JD, Jenkins AJ: Systemic and vascular inflammation is elevated in early IgA and type 1 diabetic nephropathies and relates to vascular disease risk factors and renal function. *Nephrol Dial Transplant* 20: 2420–2426, 2005
33. Yan X, Sano M, Lu L, Wang W, Zhang Q, Zhang R, Wang L, Chen Q, Fukuda K, Shen W: Plasma concentrations of osteopontin, but not thrombin-cleaved osteopontin, are associated with the presence and severity of nephropathy and coronary artery disease in patients with type 2 diabetes mellitus. *Cardiovasc Diabetol* 9: 70, 2010
34. Bidder M, Shao JS, Charlton-Kachigian N, Loewy AP, Semenkovich CF, Towler DA: Osteopontin transcription in aortic vascular smooth muscle cells is controlled by glucose-regulated upstream stimulatory factor and activator protein-1 activities. *J Biol Chem* 277: 44485–44496, 2002
35. Matsushita Y, Ogawa D, Wada J, Yamamoto N, Shikata K, Sato C, Tachibana H, Toyota N, Makino H: Activation of peroxisome proliferator-activated receptor delta inhibits streptozotocin-induced diabetic nephropathy through anti-inflammatory mechanisms in mice. *Diabetes* 60: 960–968, 2011
36. Calkin AC, Tontonoz P: Liver x receptor signaling pathways and atherosclerosis. *Arterioscler Thromb Vasc Biol* 30: 1513–1518, 2010
37. Wu J, Zhang Y, Wang N, Davis L, Yang G, Wang X, Zhu Y, Breyer MD, Guan Y: Liver X receptor-alpha mediates cholesterol efflux in glomerular mesangial cells. *Am J Physiol Renal Physiol* 287: F886–F895, 2004
38. Zhang Y, Zhang X, Chen L, Wu J, Su D, Lu WJ, Hwang MT, Yang G, Li S, Wei M, Davis L, Breyer MD, Guan Y: Liver X receptor agonist TO-901317 upregulates SCD1 expression in renal proximal straight tubule. *Am J Physiol Renal Physiol* 290: F1065–F1073, 2006
39. Morello F, de Boer RA, Steffensen KR, Gnecchi M, Chisholm JW, Boomsma F, Anderson LM, Lawn RM, Gustafsson JA, Lopez-Ilasaca M, Pratt RE, Dzau VJ: Liver X receptors alpha and beta regulate renin expression in vivo. *J Clin Invest* 115: 1913–1922, 2005
40. Mitro N, Vargas L, Romeo R, Koder A, Saez E: T0901317 is a potent PXR ligand: Implications for the biology ascribed to LXR. *FEBS Lett* 581: 1721–1726, 2007
41. Houck KA, Borchert KM, Hepler CD, Thomas JS, Bramlett KS, Michael LF, Burris TP: T0901317 is a dual LXR/FXR agonist. *Mol Genet Metab* 83: 184–187, 2004

42. Kumar N, Solt LA, Conkright JJ, Wang Y, Istrate MA, Busby SA, Garcia-Ordonez RD, Burris TP, Griffin PR: The benzenesulfoamide T0901317 [N-(2,2,2-trifluoroethyl)-N-[4-[2,2,2-trifluoro-1-hydroxy-1-(trifluoromethyl) ethyl]phenyl]-benzenesulfonamide] is a novel retinoic acid receptor-related orphan receptor-alpha/gamma inverse agonist. *Mol Pharmacol* 77: 228–236, 2010
43. Proctor G, Jiang T, Iwahashi M, Wang Z, Li J, Levi M: Regulation of renal fatty acid and cholesterol metabolism, inflammation, and fibrosis in Akita and OVE26 mice with type 1 diabetes. *Diabetes* 55: 2502–2509, 2006
44. Joseph SB, Laffitte BA, Patel PH, Watson MA, Matsukuma KE, Walczak R, Collins JL, Osborne TF, Tontonoz P: Direct and indirect mechanisms for regulation of fatty acid synthase gene expression by liver X receptors. *J Biol Chem* 277: 11019–11025, 2002
45. Ide T, Shimano H, Yoshikawa T, Yahagi N, Amemiya-Kudo M, Matsuzaka T, Nakakuki M, Yatoh S, Iizuka Y, Tomita S, Ohashi K, Takahashi A, Sone H, Gotoda T, Osuga J, Ishibashi S, Yamada N: Cross-talk between peroxisome proliferator-activated receptor (PPAR) alpha and liver X receptor (LXR) in nutritional regulation of fatty acid metabolism. II. LXRs suppress lipid degradation gene promoters through inhibition of PPAR signaling. *Mol Endocrinol* 17: 1255–1267, 2003
46. Chisholm JW, Hong J, Mills SA, Lawn RM: The LXR ligand T0901317 induces severe lipogenesis in the db/db diabetic mouse. *J Lipid Res* 44: 2039–2048, 2003
47. Miao B, Zondlo S, Gibbs S, Cromley D, Hosagrahara VP, Kirchgessner TG, Billheimer J, Mukherjee R: Raising HDL cholesterol without inducing hepatic steatosis and hypertriglyceridemia by a selective LXR modulator. *J Lipid Res* 45: 1410–1417, 2004
48. Cha JY, Repa JJ: The liver X receptor (LXR) and hepatic lipogenesis. The carbohydrate-response element-binding protein is a target gene of LXR. *J Biol Chem* 282: 743–751, 2007
49. Caldas YA, Giral H, Cortázar MA, Sutherland E, Okamura K, Blaine J, Sorribas V, Koepsell H, Levi M: Liver X receptor-activating ligands modulate renal and intestinal sodium-phosphate transporters. *Kidney Int* 80: 535–544, 2011
50. Okada S, Shikata K, Matsuda M, Ogawa D, Usui H, Kido Y, Nagase R, Wada J, Shikata Y, Makino H: Intercellular adhesion molecule-1-deficient mice are resistant against renal injury after induction of diabetes. *Diabetes* 52: 2586–2593, 2003
51. Agnihotri R, Crawford HC, Haro H, Matrisian LM, Havrda MC, Liaw L: Osteopontin, a novel substrate for matrix metalloproteinase-3 (stromelysin-1) and matrix metalloproteinase-7 (matrilysin). *J Biol Chem* 276: 28261–28267, 2001

This article contains supplemental material online at http://jasn.asnjournals.org/lookup/suppl/doi:10.1681/ASN.2012010022/-/DCSupplemental

Anal Bioanal Chem
DOI 10.1007/s00216-012-6412-x

ORIGINAL PAPER

Metabolic profiling reveals new serum biomarkers for differentiating diabetic nephropathy

Akiyoshi Hirayama · Eitaro Nakashima · Masahiro Sugimoto · Shin-ichi Akiyama · Waichi Sato · Shoichi Maruyama · Seiichi Matsuo · Masaru Tomita · Yukio Yuzawa · Tomoyoshi Soga

Received: 2 July 2012 / Revised: 4 September 2012 / Accepted: 5 September 2012

Abstract Capillary electrophoresis coupled with time-of-flight mass spectrometry was used to explore new serum biomarkers with high sensitivity and specificity for diabetic nephropathy (DN) diagnosis, through comprehensive analysis of serum metabolites with 78 diabetic patients. Multivariate analyses were used for identification of marker candidates and development of discriminative models. Of the 289 profiled metabolites, orthogonal partial least-squares discriminant analysis identified 19 metabolites that could distinguish between DN with macroalbuminuria and diabetic patients without albuminuria. These identified metabolites included creatinine, aspartic acid, γ-butyrobetaine, citrulline, symmetric dimethylarginine (SDMA), kynurenine, azelaic acid, and galactaric acid. Significant correlations between all these metabolites and urinary albumin-to-creatinine ratios ($p<0.009$, Spearman's rank test) were observed. When five metabolites (including γ-butyrobetaine, SDMA, azelaic acid and two unknowns) were selected from 19 metabolites and applied for multiple logistic regression model, AUC value for diagnosing DN was 0.927 using the whole dataset, and 0.880 in a cross-validation test. In addition, when four known metabolites (aspartic acid, SDMA, azelaic acid and galactaric acid) were applied, the resulting AUC was still high at 0.844 with the whole dataset and 0.792 with cross-validation. Combination of serum metabolomics with multivariate analyses enabled accurate discrimination of DN patients. The results suggest that capillary electrophoresis-mass spectrometry based metabolome analysis could be used for DN diagnosis.

Keywords Diabetic nephropathy · Capillary electrophoresis-mass spectrometry · Metabolome · Biomarker · Multiple logistic regression · Orthogonal partial least-squares discriminant analysis

A. Hirayama · M. Sugimoto · M. Tomita · T. Soga (✉)
Institute for Advanced Biosciences, Keio University,
246-2 Mizukami, Kakuganji,
Tsuruoka, Yamagata 997-0052, Japan
e-mail: soga@sfc.keio.ac.jp

E. Nakashima
Japan Labour Health and Welfare Organization Chubu Rosai Hospital,
1-10-6 Koumei-cho, Minato-ku,
Nagoya, Aichi 455-8530, Japan

E. Nakashima
Department of Endocrinology and Diabetes, Nagoya University Graduate School of Medicine,
65 Tsurumai-cho, Showa-ku,
Nagoya, Aichi 466-8550, Japan

M. Sugimoto
Medical Innovation Center, Kyoto University Graduate School of Medicine,
Yoshida Konoe, Sakyo-ku,
Kyoto 606-8501, Japan

S.-i. Akiyama · W. Sato · S. Maruyama · S. Matsuo · Y. Yuzawa
Department of Nephrology of Internal Medicine, Nagoya University Graduate School of Medicine,
65 Tsurumai-cho, Showa-ku,
Nagoya, Aichi 466-8550, Japan

Introduction

Diabetic nephropathy (DN) is one of the major complications of diabetes mellitus (DM) and has become the most prevalent cause of end-stage renal disease worldwide [1]. DN is also one of the most significant long-term diseases in terms of morbidity and mortality for individuals with diabetes [2]. Recent

Published online: 29 September 2012

studies have shown that several interventions can slow the progression of DN, and their impact is greater if they are started at an early stage of the development of nephropathy [3]. Although renal biopsy is the most accurate diagnostic method for DN, routine renal biopsies are not acceptable in current clinical practice because of their invasiveness. Microalbuminuria is an alternative, non-invasive marker that can be used for DN risk assessment, and the urinary albumin-to-creatinine ratio (UACR) on first-void urine sample is recommended for DN screening. However, large prospective studies have revealed poor accuracy of this marker, even though urine samples are collected two or three times a day to normalize day-to-day variation [4]. Therefore, identifying reliable and versatile biomarkers for risk assessment of DN is important.

Mass spectrometry-based urinary proteomics is used for biomarker discoveries of DN. Dihazi et al. used surface-enhanced laser desorption/ionization time-of-flight mass spectrometry to identify three urinary proteins that differentiated patients with DN from patients with type 2 DM without nephropathy, patients with type 2 DM with micro- or macroalbuminuria, patients with proteinuria caused by non-diabetic renal disease, and healthy controls [5]. Mischak et al. profiled urinary polypeptides using capillary electrophoresis-mass spectrometry (CE-MS) and found that the MS patterns could be used to differentiate type 2 DM from healthy controls [6]. However, urinary protein markers sometimes show a wider variation than blood samples. Thus, it is necessary to discover biomarkers with small diurnal variations.

Metabolomics is the comprehensive analysis of low weight molecules in a sample, and has become a powerful tool in the biomarker discovery field. Nuclear magnetic resonance [7], gas chromatography-mass spectrometry [8], liquid chromatography-mass spectrometry (LC-MS; [9]), and CE-MS [10–12] are currently used for metabolomics. Targeted profiling, that is, detection of only a few sets of metabolites, has been used to discover biomarkers for DN. Xia et al. analyzed six intermediate metabolites of the purine degradation pathway in plasma from patients with non-DN and DN using LC with or without MS [13]. They found that adenosine, inosine, uric acid, and xanthine were useful biomarkers for monitoring DM progression. Jiang et al. used LC-tandem mass spectrometry to simultaneously quantify eight aminothiols in the homocysteine metabolic cycle in plasma and found two sulfur-containing metabolites, *S*-adenosylmethionine and *S*-adenosylhomocysteine, as potential biomarkers for DM and DN [14].

Compared to targeted profiling, comprehensive metabolome analysis of all metabolites in the given sample is a more powerful technique. Zhang et al. used non-targeted LC-MS to detect potential biomarker candidates of DN and type 2 DM, and observed significant differences in the serum levels of leucine, dihydrosphingosine, and phytosphingosine [15]. However, there are few published comprehensive metabolome profiles of DN.

Recently, we developed a non-targeted CE-MS-based metabolome profiling technique [11, 16] and applied it to biomarker discovery for acetaminophen-induced hepatotoxicity in mice [11] and several types of cancer-specific profiles in human saliva [12]. In the present study, we used CE-MS to identify serum metabolite biomarkers for DN diagnosis. Furthermore, classification models incorporating multiple biomarkers were constructed for discriminating DN from non-DN.

Materials and methods

Sample collection and metabolite extraction

All experiments were conducted in accordance with study protocol approved by the Institutional Ethics Committee of Chubu Rosai Hospital. Informed consent was obtained from all patients according to the Declaration of Helsinki as revised in 2000. Serum samples from 78 type 2 DM patients were collected and classified into the following three groups: DM group without nephropathy and albuminuria (non-DN, UACR<30 mg/g, n=20), early DN group with microalbuminuria (micro-DN, 30<UACR<300 mg/g, n=32), and overt DN group with macroalbuminuria (macro-DN, UACR>300 mg/g, n=26). All serum samples were stored at −80 °C.

To extract metabolites, the frozen sera samples were thawed and 100 μl aliquots were put into 900 μl of methanol that contained internal standards (20 μmol/l each of methionine sulfone and camphor 10-sulfonic acid). The internal standards were used to normalize the extraction efficiency of metabolites during sample preparation for both cationic (methionine sulfone) and anionic (camphor 10-sulfonic acid) metabolite analysis. The solutions were mixed well and then 400 μl of Milli-Q water and 1 ml of chloroform were added, followed by centrifugation at 4,600×g for 5 min at 4 °C. The aqueous layer was transferred to a 5-kDa cutoff centrifugal filter tube (Millipore, Billerica, MA, USA) to remove large molecules. The filtrate was centrifugally concentrated at 35 °C and reconstituted with 50 μl of Milli-Q water that contained reference compounds (200 μmol/l each of 3-aminopyrrolidine and trimesic acid) immediately before CE-TOFMS analysis. These reference compounds were added to eliminate the variation in migration time of individual peaks in electropherogram among multiple datasets.

Reagents

Methionine sulfone (internal standard) was purchased from Alfa Aesar (Ward Hill, MA), and hexakis-(2,2-difluoroethoxy)-phosphazene (Hexakis) from SynQuest

Laboratories (Alachua, FL). All other reagents were obtained from Sigma-Aldrich (St. Louis, MO) or Wako Pure Chemicals Industries Ltd. (Osaka, Japan). All chemicals used were of analytical or reagent grade. Water was purified with a Milli-Q purification system (Millipore, Billerica, MA).

Instruments

All CE-electrospray ionization (ESI)-TOFMS experiments were performed using an Agilent CE capillary electrophoresis system (Agilent Technologies, Waldbronn, Germany), an Agilent G3250AA LC/MSD TOF system (Agilent Technologies, Palo Alto, CA, USA), an Agilent 1100 series isocratic HPLC pump, a G1603A Agilent CE-MS adapter kit, and a G1607A Agilent CE-ESI-MS sprayer kit. The CE-MS adapter kit included a capillary cassette, which facilitated thermostating of the capillary, and the CE-ESI-MS sprayer kit, which simplified coupling of the CE system with the MS system, was equipped with an electrospray source. For system control and data acquisition, G2201AA Agilent Chemstation software was used for CE, and Agilent TOF (Analyst QS) software was used for TOFMS. The original Agilent SST316Ti stainless steel (Fe/Cr/Ni/Mo/Ti; 68:18:11:2:1) ESI needle was replaced with a platinum needle for anion analysis [17]. The resolution of the TOFMS instrument used in this study is higher than 3,000 at *m/z* 100 with high mass accuracy (<3 ppm).

CE-TOFMS analysis of cationic metabolites

CE-TOFMS analysis of cationic metabolites was performed as described previously [10]. Cationic metabolites were separated in a fused-silica capillary (50 μm i.d.×100 cm total length) filled with 1 mol/l formic acid as the reference electrolyte. The sample solution was injected at 5 kPa for 3 s (approximately 3 nl), and a positive voltage of 30 kV was applied. The capillary and sample trays were maintained at 20 °C and <5 °C, respectively. The sheath liquid was methanol/water (50 %*v*/*v*) containing 0.1 μmol/l Hexakis and was delivered at 10 μl/min. ESI-TOFMS was operated in positive ion mode. The capillary voltage was set at 4 kV, and the nitrogen gas (heater temperature 300 °C) flow rate was set at 10 l/min. In TOFMS, the fragmenter voltage, skimmer voltage, and octapole radio frequency voltage were set at 75, 50, and 125 V, respectively. An automatic recalibration function was performed using the following masses of two reference standards: [^{13}C isotopic ion of the protonated methanol dimer $(2MeOH + H)]^+$, *m/z* 66.06306; and [protonated Hexakis $(M + H)]^+$, *m/z* 622.02896. Mass spectra were acquired at a rate of 1.5 cycles per second from *m/z* 50 to 1000.

CE-TOFMS analysis of anionic metabolites

The CE-TOFMS analysis of anionic metabolites was performed as described previously [17]. Anionic metabolites were separated in a commercially available COSMO(+) capillary, which was chemically coated with a cationic polymer. Ammonium acetate solution (50 mmol/l, pH 8.5) was used as the electrolyte for CE separation. The sample solution was injected at 5 kPa for 30 s (approximately 30 nl) and a voltage of −30 kV was applied. Ammonium acetate (5 mmol/l) in methanol/water (50 %*v*/*v*) containing 0.1 μmol/l Hexakis was delivered as the sheath liquid at 10 μl/min. ESI-TOFMS was operated in negative ion mode. The capillary voltage was set at 3.5 kV. In TOFMS, the fragmenter voltage, skimmer voltage, and octapole radio frequency voltage were set at 100, 50, and 200 V, respectively. An automatic recalibration function was performed using the following masses of two reference standards: [^{13}C isotopic ion of deprotonated acetic acid dimer $(2CH_3COOH-H)]^-$, *m/z* 120.03834; and [Hexakis + deprotonated acetic acid $(M + CH_3COOH-H)]^-$, *m/z* 680.03554. Mass spectra were acquired at a rate of 1.5 cycles per second from *m/z* 50 to 1,000.

Data processing

The raw data were processed using our proprietary software (MasterHands) [10, 12]. The overall data processing flow consisted of noise filtering, baseline correction, peak detection, and integration of the peak areas from 0.02*m/z*-wide sections of the electropherograms. Subsequently, the accurate *m/z* of each peak was calculated by Gaussian curve fitting in the *m/z* domain, and the migration times were normalized to match the detected peaks among the multiple datasets. The peaks were identified by matching *m/z* values and normalized migration times of corresponding authentic standard compounds. Processed peak lists were exported for further statistical analysis.

Statistical analysis

The relative ratio of the detected peak area to that of the internal standard was used to eliminate systematic bias derived from injection volume variance and MS sensitivity. Data were analyzed with GraphPad Prism 5.0 (GraphPad Software, Inc., San Diego, CA, USA) for statistical tests. The Kruskal–Wallis test and Dunn's post test were used to assess the statistical significance of differences among non-DN, micro-DN and macro-DN samples. The Spearman's rank correlation test was used to calculate correlations among UACR, eGFR, and the relative ratios of peak areas of the metabolites. Multiple logistic regression (MLR) models were developed to discriminate non-DN and DN cohorts. Biomarker metabolites for these models were selected in

two procedures. First, normalized data were subjected to orthogonal partial least-squares discriminant analysis (OPLS-DA) using SIMCA-P + software (Version 12.0, Umetrics, Umeå, Sweden), and a model was built and used to identify marker metabolites that accounted for differentiation of non-DN and macro-DN cohorts. Next, a stepwise variable selection method (forward and backward selection) was conducted with a threshold of $p<0.25$ for adding and eliminating features using JMP 8.0 (SAS Institute Inc., Cary, NC, USA). The generalization ability of the developed MLR model was evaluated using cross-validation methods. Tenfold cross-validation was conducted 20 times with different random seeds using WEKA (ver. 3.6.1, The University of Waikato, Hamilton, New Zealand) to split the datasets into training and validation data [18]. Bootstrap analysis was also conducted to estimate the optimistic bias in the given datasets. Two hundred replicates, including the same number of patients, were computationally generated with a random selection of individuals, this permitted redundant selection, and MLR models were developed and cross-validation tests were conducted on each generated dataset.

Results

Metabolome analysis of serum samples obtained from non-DN and DN patients

Serum metabolome profiles of 78 patients in three successive stages of DN were collected using a single standard protocol [non-DN (n=20), micro-DN (n=32) and macro-DN (n=26)] and analyzed. Age distribution, gender and other clinical characteristics are listed in Table 1. The ages in the micro-DN and macro-DN groups were slightly higher than in the non-DN group (p=0.0226). The macro-DN group had significantly higher creatinine contents and lower estimated glomerular filtration rates (eGFR) than the other groups ($p<0.0001$), while no significant difference was seen between the non-DN and micro-DN groups. The macro-DN group also showed significantly higher triglycerides and systolic blood pressure (SBP) compared with the non-DN group (p=0.0172 and 0.0083, respectively). The other clinical parameters showed no significant difference among all groups ($p>0.05$).

On average, 4400 peaks were detected from each serum sample with CE-TOFMS. After eliminating redundant peaks, such as noise, fragments and adduct ions, 289 metabolites remained. Using this dataset, we firstly performed principal component analysis (PCA), but the resultant score plots of the PCA showed no unequivocal stage-specific clusters (data not shown). Next, OPLS-DA was performed to discriminate between DN patients (micro-DN and macro-DN) and non-DN patients based on the profiled metabolites. The OPLS-DA model demonstrated satisfactory separation between non-DN and micro-DN patients (Fig. 1a) using one predictive component and one orthogonal component (R^2X_{cum}=0.21, R^2Y_{cum}=0.676, $Q_{cum}{}^2$=0.179), and clear separation between non-DN and macro-DN patients (Fig. 1b) using one predictive component and three orthogonal components (R^2X_{cum}=0.353, R^2Y_{cum}=0.946, $Q_{cum}{}^2$=0.599). These results indicate that serum metabolome profile can be used to distinguish DN patients from non-DN patients.

The resultant S plot of the developed OPLS-DA model between non-DN and macro-DN patients identified 19 metabolites (Table 2) that were highly correlated in the separation of the groups ($|p(corr)|>0.5$). Of these, we were able to assign metabolite identities to eight metabolites by matching their m/z values and migration times with those of standard reagents. These metabolites were creatinine, aspartic acid, γ-butyrobetaine, citrulline, symmetric dimethylarginine (SDMA), kynurenine, azelaic acid, and galactaric acid. The composition formulae of the other metabolites were calculated based on their isotope distribution patterns as follows: $C_5H_8N_2O_2$ [metabolite ID (MID) 17], $C_9H_{17}NO$ (MID 51), $C_9H_{19}NO$ (MID 52), $C_2H_4N_2O_3$ (MID 158), and $C_6H_6N_4O$ (MID 202). Only the m/z values of the other metabolites are listed in Table 2 because of insufficient isotope peak size. The AUC values of MID 202 (0.765, 95 % CI); 0.649–0.880, $p=4.47\times10^{-4}$) gave the best discriminating ability among these markers (Table 3).

Correlation between biomarker candidates and clinical parameters

Correlation analysis between these 19 serum biomarker candidates and currently available clinical parameters showed all candidate metabolites were significantly correlated with UACR ($p<0.009$) (Table 4). The correlation coefficients for creatinine (r=0.5701), aspartic acid (r=0.4993), γ-butyrobetaine (r=0.4942), citrulline (r=0.4300), SDMA (r=0.4820), kynurenine (r=0.5351), MID 17 (r=0.4968), MID 97 (r=0.5223), MID 152 (r=0.5336), MID 158 (r=0.4980), and MID 202 (r=0.6352) were positively correlated with UACR. Those of azelaic acid (r=–0.5210), galactaric acid (r=–0.4596), MID 51 (r=–0.4728), MID 52 (r=–0.4871), MID 96 (r=–0.3085), MID 114 (r=–0.3638), MID 127 (r=–0.2961), and MID 134 (r=–0.3669) were negatively correlated. Furthermore, 15 of 19 metabolites were significantly correlated with eGFR ($p<0.035$). The correlation coefficients of creatinine (r=–0.8832), aspartic acid (r=–0.3912), γ-butyrobetaine (r=–0.6492), citrulline (r=–0.6531), SDMA (r=–0.7111), kynurenine (r=–0.5627), MID 17 (r=–0.5808), MID 97 (r=–0.7651), MID 152 (r=–0.7687), MID 158 (r=–0.6302), and MID

Table 1 Clinical characteristics of diabetic nephropathy patients

	Non-DN	Micro-DN	Macro-DN	*p* value
Number	20	32	26	
Male/Female	9/11	22/10	17/9	
Age (years)	57.5±12.9	66.6±9.2[a]	67.3±8.7[a]	0.0226
BMI (kg/m^2)	26.9±5.0	24.6±3.4 (1)	24.8±3.0	0.3074
HbA_{1c} (%)	6.8±1.0	7.2±1.1	6.8±0.7	0.3931
UACR (mg/g)	12.1±6.7	103.9±77.8[a]	1055.3±741.3[a, b]	<0.0001
Creatinine (enzymatic, mg/dL)	0.71±0.18	0.84±0.28	1.39±0.66[a,b]	<0.0001
Triglycerides (mg/dL)	134.6±131.5	133.5±55.2	179.7±110.3[a] (3)	0.0172
Cholesterol (mg/dL)	190.4±53.5 (2)	198.5±25.7 (2)	218.0±41.9 (1)	0.0838
HDL cholesterol (mg/dL)	56.3±18.9	50.9±14.6	52.9±21.1 (1)	0.5011
LDL cholesterol (mg/dL)	120.4±31.7	120.5±26.2 (1)	125.8±34.1 (1)	0.8421
Systolic BP (mmHg)	132±21	143±23	152±22[a]	0.0083
Diastolic BP (mmHg)	74±13	79±14	81±10	0.0711
eGFR (mL/min/1.73 m^2)	81.9±24.0	70.5±21.9	47.2±25.6[a,b]	<0.0001
Medication (number)				
Diabetic drug	17	27	25	
Hypolipidemic drug	10	16	14	
Antihypertensive drug	10	19	22	

The number in parentheses indicates the number of patients for which clinical values were missing. The *p* values were calculated using the data from the patients without missing values. Data are means±SD

[a]Significantly different compared to non-DN group

[b]Significantly different compared to micro-DN group

202 (r=–0.7455) showed negative correlation with eGFR. This indicates that they were positively associated with renal dysfunction. By contrast, those of azelaic acid (r=0.3739), galactaric acid (r=0.4152), MID 51 (r=0.2204), and MID 134 (r=0.2397) showed positive correlation with eGFR.

MLR model development

For the discrimination of DN (micro-DN and macro-DN) from non-DN patients, we developed a MLR model. Of the 19 biomarker candidates, γ-butyrobetaine, SDMA, azelaic acid, MID 114, and MID 127 were selected by stepwise feature selection as MLR variables. The developed model yielded high AUC values (0.927, 95 % CI, 0.870–0.983, p< 0.0001, Fig. 2a). The model also yielded high AUC values (±SD; 0.880±8.62×10^{-3}) in the cross-validation test. In a bootstrap test, the AUC values were 0.946±0.0262 and 0.895±0.0364 for training and cross-validation, respectively. To evaluate only the eight identified metabolites, we independently developed a MLR model. Stepwise feature selection selected aspartic acid, SDMA, azelaic acid, and galactaric acid as MLR variables. This MLR model also yielded high AUC values (0.844, 95 % CI, 0.754–0.934, p<0.0001, Fig. 2b), although it performed slightly worse than the model with all metabolites, including unknown peaks. This model also yielded high AUC values (±SD;

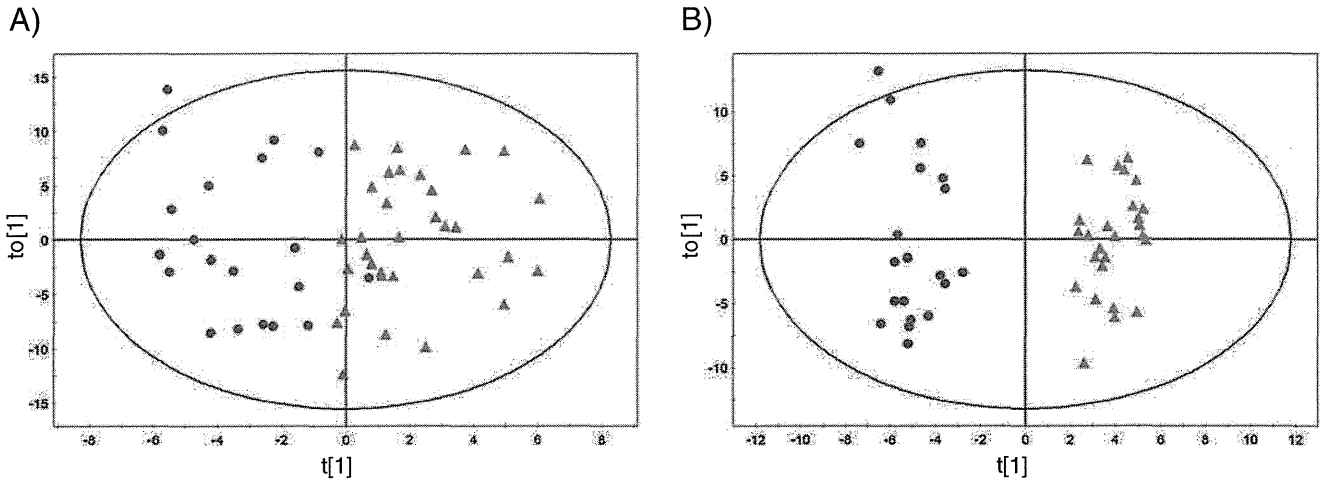

Fig. 1 OPLS-DA based on comprehensive metabolites data from (**A**) non-DN (*blue dots*) and micro-DN (*pink triangles*) samples and (**B**) non-DN (*blue dots*) and macro-DN (*red triangles*) samples. The *ellipse* in each figure indicates the Hotelling T2 (0.95) range for this model

Table 2 The 19 serum biomarker candidates that statistically differentiated the different DN stages

MID	Mode[a]	*m/z*	Non-DN	Micro-DN	Macro-DN	*p* value	Formula	Metabolite
11	C	114.067	0.501±0.153	0.612±0.209	1.052±0.506	<0.0001	$C_4H_7N_3O$	Creatinine
17	C	129.067	0.046±0.035	0.065±0.049	0.125±0.079	<0.0001	$C_5H_8N_2O_2$	
29	C	134.046	0.126±0.025	0.141±0.041	0.170±0.036	<0.0001	$C_4H_7NO_4$	Aspartic acid
39	C	146.118	0028±0.007	0.032±0.008	0.039±0.010	<0.0001	$C_7H_{16}NO_2$	γ-Butyrobetaine
51	C	156.139	0.006±0.005	0.005±0.004	0.001±0.003	0.0005	$C_9H_{17}NO$	
52	C	158.154	0.063±0.020	0.055±0.022	0.040±0.012	0.0007	$C_9H_{19}NO$	
69	C	176.104	0.194±0.053	0.199±0.060	0.275±0.081	0.0005	$C_6H_{13}N_3O_3$	Citrulline
78	C	203.150	0.006±0.002	0.007±0.002	0.010±0.005	0.0004	$C_8H_{18}N_4O_2$	SDMA
82	C	209.093	0.010±0.004	0.011±0.005	0.016±0.005	0.0002	$C_{10}H_{12}N_2O_3$	Kynurenine
96	C	243.184	0.026±0.013	0.019±0.012	0.015±0.007	0.0301		
97	C	244.106	0.0006±0.001	0.0009±0.001	0.002±0.002	0.0003		
114	C	276.128	0.008±0.006	0.006±0.004	0.003±0.003	0.0104		
127	C	302.197	0.106±0.050	0.079±0.047	0.062±0.028	0.0372		
134	C	316.213	0.010±0.009	0.006±0.007	0.003±0.002	0.0158		
152	A	96.960	0.216±0.063	0.243±0.063	0.341±0.103	<0.0001		
158	A	103.014	0.003±0.002	0.004±0.002	0.005±0.002	0.0001	$C_2H_4N_2O_3$	
202	A	149.049	0.030±0.006	0.034±0.009	0.051±0.019	<0.0001	$C_6H_6N_4O$	
232	A	187.098	0.020±0.013	0.017±0.011	0.009±0.004	<0.0001	$C_9H_{16}O_4$	Azelaic acid
246	A	209.031	0.029±0.012	0.024±0.009	0.016±0.013	<0.0001	$C_6H_{10}O_8$	Galactaric acid

[a] Mode "C" and "A" indicate that the candidate metabolites were obtained in cationic and anionic analysis, respectively

The relative ratio of peak area of each metabolite is shown as the mean±SD

$0.792\pm1.21\times10^{-2}$) in the cross-validation test. In a bootstrap test, the AUCs were 0.875±0.0419 and 0.820±0.0543 for training and cross-validation, respectively. These results indicate that the developed model is sufficiently accurate, specific, and general.

Table 3 AUC values for individual markers

Metabolite	AUC	95 % CI		*p* value
Creatinine	0.7526	0.6423	0.8629	8.06×10^{-4}
MID 17	0.7319	0.6128	0.851	2.09×10^{-3}
Aspartic acid	0.7069	0.5871	0.8267	6.05×10^{-3}
γ–Butyrobetaine	0.7379	0.6149	0.8609	1.60×10^{-3}
MID 51	0.644	0.5021	0.7858	0.0561
MID 52	0.7078	0.5853	0.8302	5.84×10^{-3}
Citrulline	0.6431	0.5158	0.7704	0.0576
SDMA	0.731	0.6098	0.8522	2.18×10^{-3}
Kynurenine	0.7284	0.6122	0.8447	2.44×10^{-3}
MID 96	0.6828	0.5475	0.818	0.0153
MID 97	0.6655	0.5396	0.7914	0.0281
MID 114	0.6836	0.5399	0.8274	0.0148
MID 127	0.6707	0.5321	0.8093	0.0235
MID 134	0.6552	0.5102	0.8001	0.0395
MID 152	0.7302	0.6048	0.8555	2.26×10^{-3}
MID 158	0.7108	0.5809	0.8407	5.16×10^{-3}
MID 202	0.7647	0.6492	0.8801	4.47×10^{-4}
Azelaic acid	0.731	0.6151	0.8469	2.18×10^{-3}
Galactaric acid	0.7591	0.6169	0.9012	5.89×10^{-4}

Discussion

The aim of this study was to obtain metabolic markers for early detection of DN from patient serum samples. We used CE-MS-based metabolome analysis to find differences in the serum metabolites from non-DN, micro-DN, and macro-DN samples. OPLS-DA with 289 metabolites clearly separated non-DN from macro-DN. Adequate separation of micro-DN from non-DN was also achieved. These results show that OPLS-DA is useful in this type of analysis. The resultant S-plot of the developed OPLS-DA model identified 19 metabolites that were major contributors to the separation of macro-DN from non-DN ($|p(corr)|>0.5$). These metabolites showed a gradual increase or decrease with progressive development of nephropathy. Among them, eight metabolites were identified, and these markers are discussed in comparison with other published reports below.

The concentration of serum creatinine was significantly increased in the micro-DN and macro-DN groups compared with the non-DN group ($p<0.0001$), and positively correlated with UACR ($r=0.5701$, $p<0.0001$) and negatively correlated

Table 4 Correlation analysis between the 19 biomarker candidates and clinical parameters (urinary albumin-to-creatinine ratio (UACR) or estimated glomerular filtration rate (eGFR))

MID	Metabolite	UACR		eGFR	
		Coefficients	*p* value	Coefficients	*p* value
11	Creatinine	0.5701	<0.0001[a]	−0.8832	<0.0001[a]
17		0.4968	<0.0001[a]	−0.5808	<0.0001[a]
29	Aspartic acid	0.4993	<0.0001[a]	−0.3912	0.0004[a]
39	γ-Butyrobetaine	0.4942	<0.0001[a]	−0.6492	<0.0001[a]
51		0.4728	<0.0001[a]	0.2204	<0.0001[a]
52		−0.4871	<0.0001[a]	−0.0678	0.053
69	Citrulline	0.4300	<0.0001[a]	−0.6531	<0.0001[a]
78	SDMA	0.4820	<0.0001[a]	−0.7111	<0.0001[a]
82	Kynurenine	0.5351	<0.0001[a]	−0.5627	<0.0001[a]
96		−0.3085	0.006[b]	0.1975	0.083
97		0.5223	<0.0001[a]	−0.7651	<0.0001[a]
114		−0.3638	0.001[b]	0.1392	0.224
127		−0.2961	0.009[b]	0.2035	0.074
134		−0.3669	0.001[a]	0.2397	0.035[c]
152		0.5336	<0.0001[a]	−0.7687	<0.0001[a]
158		0.4980	<0.0001[a]	−0.6302	<0.0001[a]
202		0.6352	<0.0001[a]	−0.7455	<0.0001[a]
232	Azelaic acid	−0.5210	<0.0001[a]	0.3739	0.0007[a]
246	Galactaric acid	−0.4596	<0.0001[a]	0.4152	0.0002[a]

[a] $p<0.001$
[b] $p<0.01$
[c] $p<0.05$

with eGFR (r=–0.8832, $p<0.0001$). Accumulation of serum creatinine was also observed in DN patients by metabolic analysis [19]. In clinical practice, creatinine is widely used as a marker of DN that reflects the renal function. Although serum creatinine had high specificity for detecting decreased GFR, the sensitivity is not sufficient because its levels do not significantly increase until the GFR is reduced to less than 50 % of normal levels [20].

The levels of amino acids, including aspartic acid ($p<0.0001$), citrulline (p=0.0005), SDMA (p=0.0004), and kynurenine (p=0.0002), were significantly elevated in the DN groups compared with the non-DN group. These metabolites showed high positive correlations with UACR (aspartic acid, r=0.4993, $p<0.0001$; citrulline, r=0.4300, $p<0.0001$; SDMA, r=0.4820, $p<0.0001$; kynurenine, r=0.5351, $p<0.0001$) and negative correlations with eGFR (aspartic acid, r=–0.3912, p=0.0004; citrulline, r=–0.6531, $p<0.0001$; SDMA, r=–0.7111, $p<0.0001$; kynurenine, r=–0.5627, $p<0.0001$). Aspartic acid and citrulline are involved in the urea cycle. Urea, is a major end product of

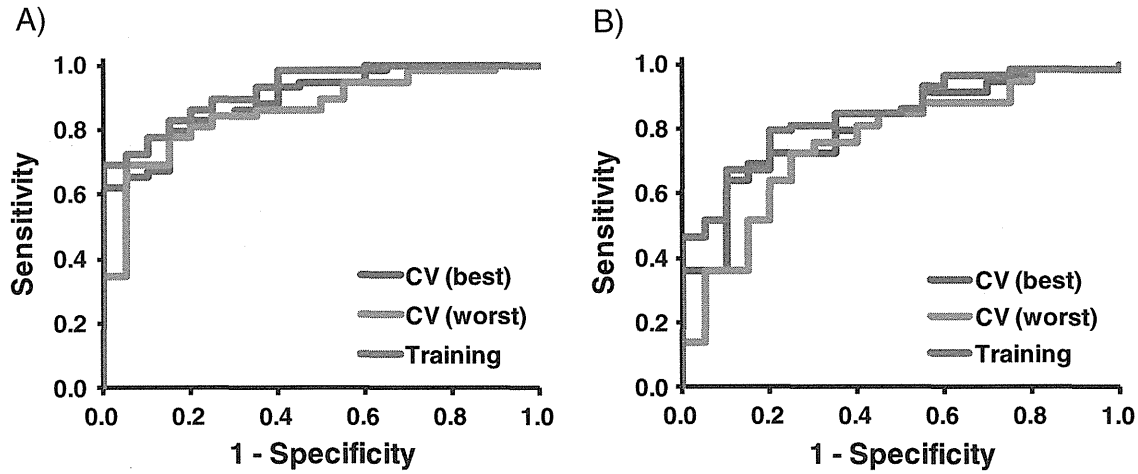

Fig. 2 ROC curve analyses in combination with (**A**) γ-butyrobetaine, SDMA, azelaic acid, MID 114, and MID 127, and (**B**) aspartic acid, SDMA, azelaic acid, and galactaric acid to discriminate non-DN and DN patients

nitrogen metabolism, and is produced by free ammonia and aspartic acid. Citrulline is normally taken up by the kidneys and converted to urea via arginine. Chuang et al. found significant accumulation of urea cycle intermediates in the patients with end-stage renal disease [21]. Because the kidneys are important in conversion of citrulline to arginine, the increase in the serum level of citrulline in DN patients could be attributed to degradation of this function.

SDMA and asymmetric dimethylarginine (ADMA), which is a structural isomer of SDMA, are formed by the enzymatic methylation of arginine residues within proteins. These metabolites have been identified as biomarkers for chronic kidney disease [22]. ADMA is metabolized by dimethylarginine dimethylaminohydrolase (EC 3.5.3.18) into citrulline and dimethylamine in the kidneys, whereas SDMA is excreted directly into the urine without further modification [23]. In this study, ADMA was under the detection limit, but SDMA was positively correlated with a decrease in function of kidney. Therefore, SDMA is a more sensitive marker than ADMA of various renal diseases, including DN.

Tryptophan is metabolized to kynurenine and further metabolized to acetyl-CoA and NAD in the tryptophan-kynurenine pathway. The rate limiting enzymes of this pathway are indoleamine 2,3-dioxygenase (EC 1.13.11.52) in the kidney and tryptophan 2,3-dioxygenase (EC 1.13.11.11) in the liver. Both these enzymes metabolize tryptophan to *N*-formylkynurenine, and *N*-formylkynurenine is subsequently catabolized to kynurenine. Saito et al. showed the peripheral kynurenine pathway accelerates in renal insufficient rats, and the reaction rate was positively correlated with the severity of the case [24]. They also found increased serum kynurenine concentrations reflected increased tryptophan 2,3-dioxygenase and decreased kynureninase (EC 3.7.1.3) activity in the liver [24]. Integration of profiling of these enzyme activities and metabolites will increase understanding of these mechanisms.

We detected a significant increase in γ-butyrobetaine in DN patients ($p<0.0001$). Toyohara et al. showed a negative correlation between γ-butyrobetaine and eGFR in plasma from the patients with chronic kidney disease [25]. Because γ-butyrobetaine is converted to L-carnitine by γ-butyrobetaine dioxygenase (EC 1.14.11.1), it is assumed the increased γ-butyrobetaine arises from inhibition of this enzyme in the kidney.

The levels of azelaic acid ($p<0.0001$) and galactaric acid ($p<0.0001$) were significantly lower in the DN groups than the non-DN group. These metabolites also showed high negative correlations with UACR (azelaic acid, $r=-0.5210$, $p<0.0001$; galactaric acid, $r=-0.4596$, $p<0.0001$) and positive correlations with eGFR (azelaic acid, $r=0.3739$, $p=0.0007$; galactaric acid, $r=0.4152$, $p=0.0002$). Azelaic acid is a saturated C9 dicarboxylic acid derived from oxidation of fatty acids and inhibits the generation of reactive oxygen species on neutrophils [26]. Galactaric acid, is a natural product found in various fruits, and acts as a growth substrate for many organisms, including *Escherichia coli* [27]. However, biological mechanisms of decreased serum azelaic acid and galactaric acid after onset DN need to be clarified.

In this study, the obtained 19 metabolites showed relatively high separation abilities (AUC values of receiver operating characteristic curves 0.643–0.765, Table 3). To increase the separation ability, we then applied a MLR model to this dataset. The developed MLR model included five metabolites, γ-butyrobetaine, SDMA, azelaic acid, MID 114, and MID 127. This model had a higher AUC value for diagnosis of DN (0.927, $p<0.0001$) than single markers, and shows the use of multiple markers is advantageous (Fig. 2a). However, this model contained two unidentified metabolites. The model using only identified metabolites was even simpler and more versatile for actual diagnosis because it could be used with quantification by another technique, such as LC, LC-MS, or an enzymatic method. Thus, we developed another MLR model using only the identified metabolites, aspartic acid, SDMA, azelaic acid and galactaric acid (Fig. 2b). This model showed high separation ability (AUC value 0.844, $p<0.0001$), and could also be used to diagnose DN. However, there are several limitations to be acknowledged for this study. For example, the developed model should be further validated using larger and independent new datasets. In addition, although we evaluated the generalization ability of the developed model using cross-validation, the specificity of the model was not assessed. Especially, the specificity for DN using data obtained from study of other kidney diseases (e.g., kidney cancer) should be addressed in future study.

In conclusion, we applied CE-MS-based metabolome profiling to serum samples from diabetic patients with or without existing DN. Biomarker candidates for the early diagnosis of DN were obtained. Although a further validation study is needed, this technique has potential as a tool for biomarker discovery studies.

Acknowledgments We thank Dr. Astuko Watarai, Japan Labour Health and Welfare Organization Chubu Rosai Hospital, for assistance with sample collection. We also thank Maki Sugawara and Hiroko Ueda, Institute for Advanced Biosciences, Keio University, and Jiro Nakamura, Department of Endocrinology and Diabetes, Nagoya University Graduate School of Medicine, for technical support and fruitful discussions. This work was supported by a Health and Labour Sciences Research Grant "Research on Biological Markers for New Drug Development", Grants from the Ministry of Health, Labour and Welfare of Japan "Research on Rare and Intractable Disease", KAKENHI Grants-in-Aid for Scientific Research on Priority Areas "Systems Genomes" and "Lifesurveyor" from the Ministry of Education, Culture, Sports, Science and Technology of Japan, and research funds from the Yamagata prefectural government and the City of Tsuruoka.